ABSTRACT

PEEPLES, CODY RYAN. Alternatives to the Americium-Beryllium Neutron Source for the Compensated Neutron Porosity Log. (Under the direction of Robin Pierce Gardner.)

Monte Carlo simulations of neutron porosity logs were performed to examine the possibility of replacing the standard Americium-Beryllium neutron source. The candidate replacement sources were the Californium-252 radioisotope and the Deuterium-Tritium fusion reaction based particle accelerator neutron source. It was found that the differences in the energy spectra of neutrons emitted by the sources made an impact on the observed response. Both candidates were found to have potential as sources for the log.

Alternatives to the Americium-Beryllium Neutron Source
for the Compensated Neutron Porosity Log

by
Cody Ryan Peeples

A thesis submitted to the Graduate Faculty of
North Carolina State University
in partial fulfillment of the
requirements for the Degree of
Master of Science

Nuclear Engineering

Raleigh, North Carolina

2007

APPROVED BY:

_____ _____
         Medhat Mickael   Roger Woodard

_____
            Robin Gardner
        Chair of Advisory Committee

DEDICATION

For the Lord and Savior of Man, Jesus, the glory of your name

For my wife Johanna and my Parents, your honor and happiness

For the men and women who fight for Liberty, your words and swords be sharp

BIOGRAPHY

I was born in Pasadena, TX on March 26, 1982 to Donna Louise Peeples and David Paul Peeples, Jr. Most of my early years were spent in Texas, and there were frequent trips to visit extended family in the delta region of the state of Mississippi from which both my parents hail.

The key formative years of what would become my future life were 1998-2000. In those years, I was enrolled in Deer Park High School, Deer Park, TX. There, I studied Physics and Calculus for the first time under the tutelage of Frank Butcher, Judy Mayer, and Shane May. In spite of previous lackluster academic accomplishments, my talent and interest in these subjects proved to be unquestionable. In 2000, I earned Deer Park High School's Most Improved Student Award and the John Christopher Patton Memorial Scholarship Award.

I entered Texas A&M University in the fall of 2000. There, I became a licensed operator of the Nuclear Science Center Nuclear Reactor at the age of 19. I also served as secretary and then president of the Texas A&M University student chapter of the American Nuclear Society. The members of the faculty that impacted me most positively were Marvin Adams, William Charlton, John Poston, Ian Hamilton, Dan Reece, and Ron Hart. I graduated with a B.S. Nuclear Engineering *cum laude* in 2004.

In the fall of 2004 I entered the NC State University Master of Science Nuclear Engineering program with the full support of the Advanced Fuel Cycle Initiative University Fellowship Program. I started out working on a project for the testing and qualification of advanced gas-cooled reactor fuels.

My first two years at NCSU were quite rocky. At the end of my first year, I felt that I needed to stand up against a situation where I thought students were being abused. I paid a very heavy price for my protest. My stand meant that I had to abandon my successful thesis work which was nearing completion, but I do not regret it.

As those events began to settle out, I chose to stay at NC State and to start over with a new thesis topic and with the general faculty's support. I chose to limit myself to subjects that would allow me to fulfill my commitment to provide the Advanced Fuel Cycle Initiative with a thesis relevant to their program. This proved to be a mistake, because the other AFCI-related projects available in the department simply did not overlap with my interests in Monte Carlo simulations and radiation detection and measurements.

In January of 2007, I finally made the difficult decision to begin again. The document you hold is the product of that decision.

ACKNOWLEDGEMENTS

TABLE OF CONTENTS

LIST OF TABLES

LIST OF FIGURES

1 Introduction

1.1 Motivation

An as of yet unpublished report titled "Radiation source use and replacement" by the National Academy Sciences (NAS) has noted potential dangers associated with the use of Americium-Beryllium (Am-Be) sources. The report notes that Am-Be sources are particularly hazardous due to the long half-life, high activity, as well as large inhalation and ingestion health risks. Am-Be sources are widely used in a well logging tool used in petroleum exploration for porosity measurements. The tool is known as the compensated neutron logging tool. In well-logging, especially in logging while drilling (LWD) operation, sources are routinely lost down-hole and the well has to be abandoned if the source is not retrieved. The body of this thesis explores the replacement of the Am-Be source with less hazardous sources for neutron porosity logging.

1.2 Background

1.2.1 Well Logging

Well logging refers to a broad class of techniques that are used chiefly in petroleum exploration for recording the properties of rock formations as a function of depth within boreholes by using a variety of sensors. Many types of sensors are commonly used including acoustic, electrical, magnetic, and nuclear (using photons and neutrons). This study is primarily concerned with neutron well logging methods which attempt to estimate the amount of hydrogen present in rock formations.

The establishment of an oil well occurs in phases. First, the borehole is drilled.

Then, piping is inserted for flow regulation and normalization. Next, shaped charges are lowered into the tube and detonated to fracture the tubing and oil bearing rock formation. Finally, pumps and valves are installed on the surface to control the well's production. Logging is usually done before the piping is inserted or before the explosive perforation. Logs may also be performed to establish the status of a well that has been producing for some time.

Well logging tools are long devices that contain sensors and sources. Traditionally they are lowered into the well after drilling, on a long wire that carries the sensor signals to log analysts on the surface. LWD tools are exposed to even greater extremes of mechanical shock and vibration than the already imposing environment of their wireline cousins. Wireline and LWD tools are expected to operate at temperatures as high as 165 °C and pressures as high as 30,000 psi. LWD tools are expected to withstand accelerations up to 200 $m/s^2 \sim 20$ "g's".

In the busy industry of petroleum exploration, logging tools must be quick and reliable. That is, they must be capable of providing information about the well while rapidly being lowered or raised in the borehole.

1.2.2 Neutrons

The neutron was first documented by Sir James Chadwick in 1932. Sir Chadwick received the Nobel Prize for his discovery in 1935. The neutron and proton are now believed to be the two types of particles that combine to make up the nucleus of all atomic structures in ordinary matter. Theory about neutron properties has led to astounding technological advances in science, industry, and medicine. Some of the astounding advances include

nuclear power, nuclear weapons, neutron radiography, neutron activation analysis, boron neutron capture therapy, and neutron well logging techniques.

The rest mass of the neutron was estimated at 939.5 MeV/c^2, which is slightly higher than the mass of the proton. As its name suggests the neutron is a neutral particle, so with few exceptions it is unaffected by electric and magnetic fields.

Neutrons are commonly classified by their kinetic energy. A typical classification is 'fast' for neutrons above 100 keV, 'intermediate' for neutrons between 1ev and 100 keV, 'epi-thermal' for neutrons between 0.1 eV and 1 eV, and 'thermal' for neutrons below 0.1 eV. The electron-Volt (eV) unit is a unit of energy that is equal to 1.6022E-19 Joules. Classification by energy is preferred because neutron behavior depends heavily on the neutron energy.

1.2.3 Neutron Sources

Neutron sources vary in intensity and in the energy of the neutrons emitted. They can be classified into three groups: nuclear fission reactors, radioisotopes, and particle accelerators. Nuclear reactors are obviously not portable, and not suitable for nuclear well logging sources. Radioisotopes are the most commonly used neutron source in well logging applications. Particle accelerators have seen relatively limited (although growing) use in well logging, and their potential to replace radioisotopes is one of the key motivations for this study.

Neutron source energy distributions for the three sources considered in this study are presented in Figure 1.

Comparison of CNL source spectra
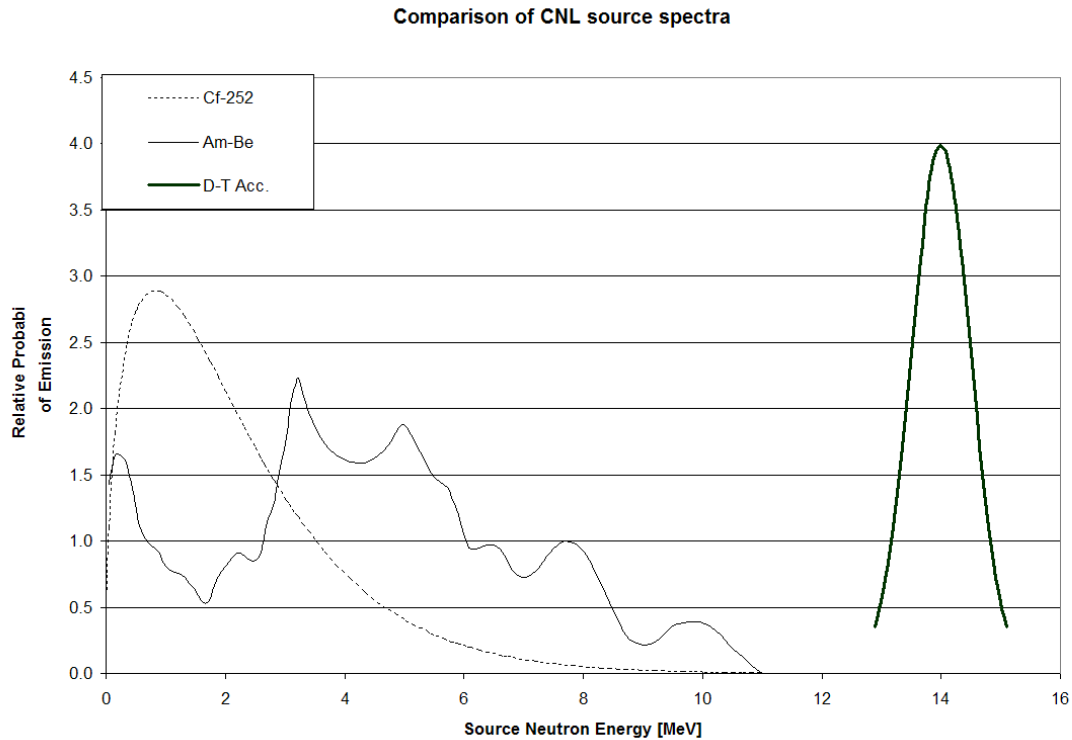
Figure 1 : Source neutron energy distributions

1.2.3a Radioisotope Neutron Sources

There are two main types of radioisotope neutron sources, direct and indirect. Direct refers to radioisotope sources that emit neutrons in their natural decay processes. Californium-252 (Cf-252) is the most widely used direct radioisotope neutron source. Cf-252 has a half life of 2.645 years, and 3.09% of decays are by spontaneous fission. The spontaneous fission decay mode is the only decay mode associated with neutron emission. On average, 3.76 neutrons are emitted per spontaneous fission event. The energy distribution of neutrons from a Californium-252 source is conveniently described by a Watts fission spectrum with an average energy of around 2.1 MeV.

4

Indirect radioisotope neutron sources refer to sources that rely on a charged particle-emitting radionuclide and a stable target nuclide to produce neutrons through a nuclear reaction. The most common indirect radioisotope neutron source is the Am-Be source. There, the alpha emitter is Americium-241 with decay energy of 5.638 MeV and a half-life of 432.2 years. The neutron producing reaction is:

$$\alpha_2^4 + Be_4^9 \rightarrow n_0^1 + C_6^{12}$$
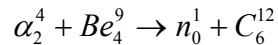
The alpha particles, emitted in Am-241 decay, impinge on a Be-9 target, producing neutrons over a broad range of energies with an average energy around 4.2 MeV and a maximum around 10 MeV (Marsh).

1.2.3b Particle Accelerator Neutron Sources

For near-term engineering applications, nuclear fusion based devices are the only feasible option for accelerator sources. Devices based on the Deuterium-Tritium fusion reaction are available that produce mono-energetic neutrons with energy around 14 MeV. These devices contain a deuterium gas reservoir, an ionizer, an accelerating potential, and a Tritium bearing target. The reaction is:

$$H_1^2 + H_1^3 \rightarrow n_0^1 + He_2^4$$
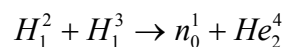
Similar devices are also available that are based on the Deuterium-Deuterium fusion reaction. The neutrons emitted in that reaction are mono-energetic at 2.2 MeV.

Both types of accelerator sources have similar problems of cost and maintenance. The Deuterium reservoir and the target material become depleted over time, and a typical operating lifetime for a D-T source is 1000-2000 hours of operation depending on output. The D-D sources have significantly lower neutron output than the D-T type, which limits their use for this application.

1.2.4 Neutron Interactions

The neutron interactions that have been studied the most are interactions of neutrons with the nuclei of atoms of ordinary elements. The typical analysis begins with a separation between absorption and scattering reactions.

In such analyses, absorption reactions include those where the neutron becomes part of the nucleus, and another type of particle is emitted. The absorption reactions most important to nuclear well logging are (n,gamma) and (n,p) reactions; where neutron absorption is followed by the emission of a gamma ray or proton, respectively.

Scattering interactions result in the neutron changing energy and/or direction. They can be elastic or inelastic. Elastic scattering is essentially a two-body collision in which energy is conserved. Neutron elastic scattering resembles a billiard ball collision, where two particles collide and the resulting change in energy and direction of the particles is a function of their masses. Therefore, scattering of a neutron from a hydrogen nucleus, which has mass almost equal to the neutron mass, presents the possibility of a neutron losing most of its kinetic energy (Duderstadt). Elastic scattering is well described by classical physics, with relativistic corrections needed for neutrons of energy above a few MeV.

However, in molecular and crystalline materials, elastic scattering from light nuclei can be complicated by inter-atomic bonds which act as shock absorbers when the neutron energy is comparable to the energy of the bonds (a few eV). Practically, these complications are handled through the use of what is known as S(alpha,beta) tables (Koppel).

Inelastic scattering involves the absorption and subsequent reemission of a neutron by a nucleus, leaving the nucleus in an excited state. There are characteristic gamma rays associated with the de-excitation of the scattering nucleus, and detection of these gamma rays has applications in nuclear well logging as well as other areas.

For compensated neutron porosity logs, the most important interactions are:

1) elastic scattering with hydrogen in the water-or-oil filled porosity of the rock

2) (n,p) reactions with He^3 in the detector volumes.

3) myriad absorption reactions that occur with greater frequency once the neutrons have been slowed down by elastic scattering.

4) inelastic scattering with nuclides of low to intermediate mass in the rock formation (e.g. C, Ca, O, Si)

Note that all of these interactions are greatly influenced by the energy of the incident neutrons.

1.2.5 Neutron Cross-Sections and Neutron Flux

Cross sections are estimates of the probability of neutron interactions. *Microscopic cross-sections* are typically given in units of barns (1 barn = 10^{-24} cm^2), and represent the cross-sectional area that a single nucleus has for a given neutron reaction. *Macroscopic cross-sections* are derived by multiplying microscopic cross-sections by the number density of the appropriate nucleus in a macroscopic material, thus arriving at an estimate of the probability per unit neutron path length of a given reaction.

The macroscopic cross section of a homogeneous mixture of nuclides is calculated by summing the products of the individual nuclide's number densities with their corresponding microscopic cross-sections. See Equation 1, where Σ is the macroscopic cross-section, N_i is the number density of nuclide i, σ_i is the microscopic cross-section of nuclide i, and n is the number of nuclides in the homogeneous material.

$$\Sigma = \sum_{i=1}^{n} N_i \sigma_i \qquad \textbf{Equation 1}$$

Differential cross-sections are sets of microscopic cross-section data that differentiate between certain aspects of the reaction that they represent. The most common form of differential cross-section gives the probability of a scattering interaction as a function of energy and the change in the neutron direction.

The neutron flux is a quantity for a given system, that when multiplied by the macroscopic neutron cross-section yields the reaction rate density [reactions/cc-s]. Neutron-path-length-rate-density [i.e. n-cm/(cm^3-s)] is a useful, if seemingly convoluted, way to think about neutron fluxes, because a macroscopic cross-section can be simply understood as the reaction probability per unit neutron-path-length. More typically the units of neutron flux are presented as [n/cm^2-s], but the units differ slightly for *angular neutron flux* and *energy-dependent neutron flux*.

Neutron cross-sections have very strong dependence on the kinetic energy of the incident neutron. A few pertinent examples are given in Figure 2 through Figure 6.
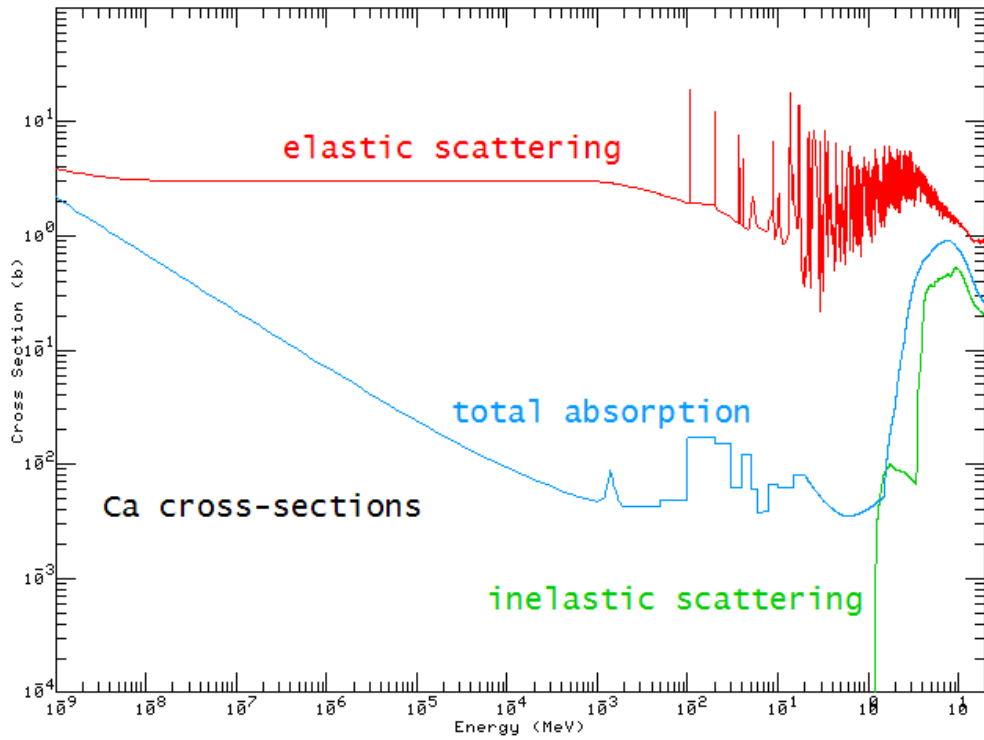
Figure 2 : ENDF/B-VI microscopic cross sections for Ca
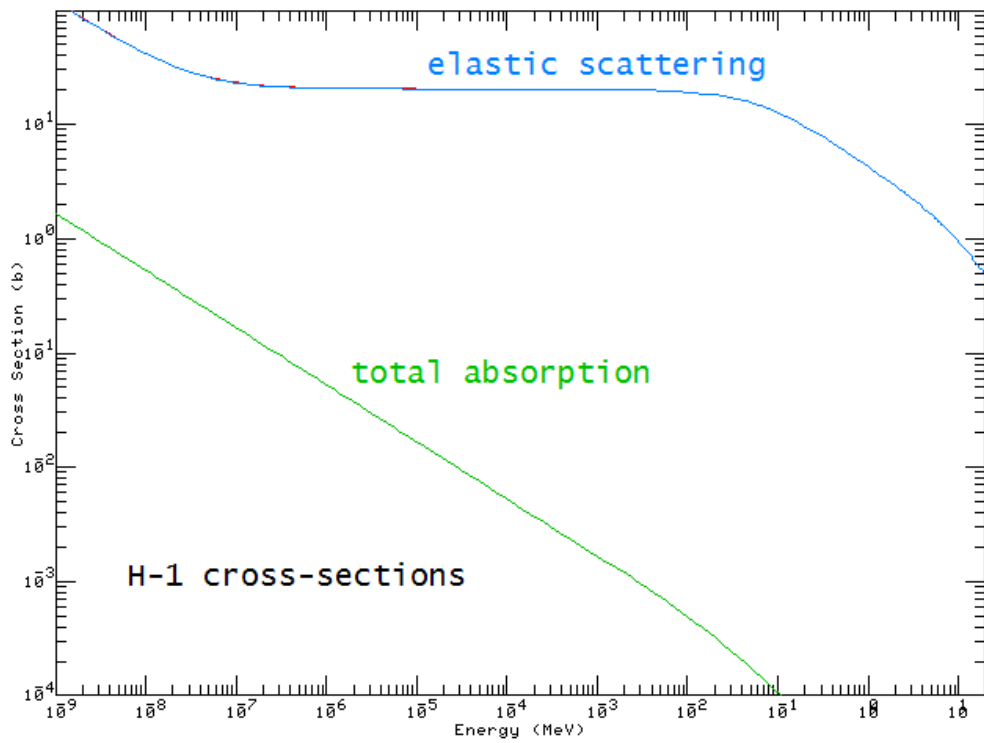
Figure 3 : ENDF/B-VI microscopic cross sections for H-1

9
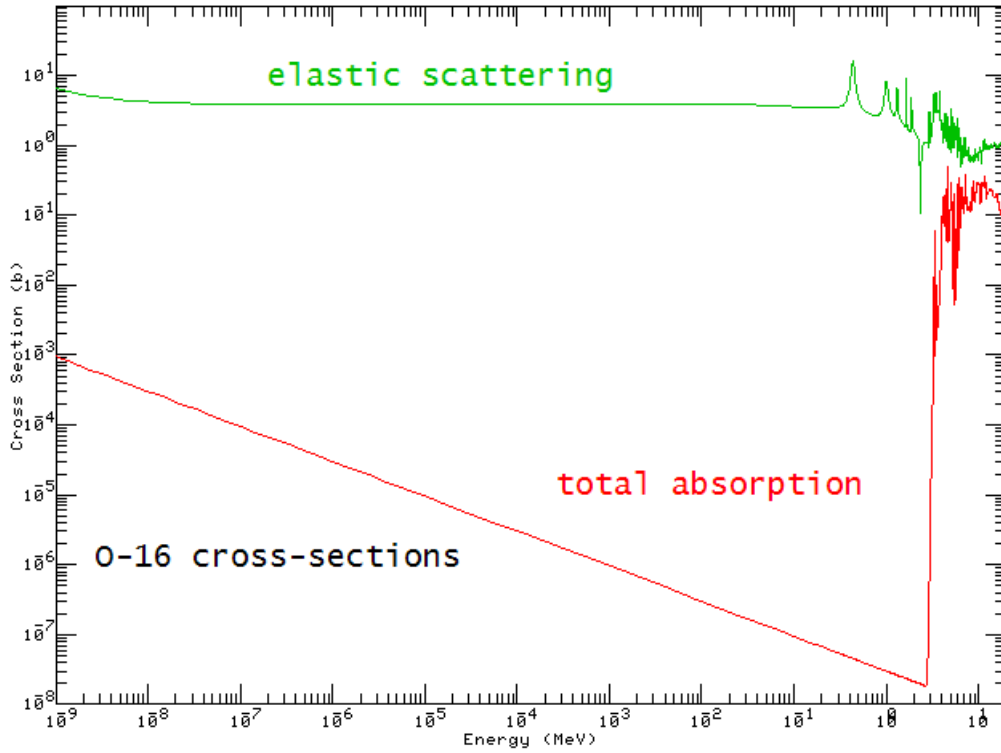
Figure 4 : ENDF/B-VI cross sections for O-16
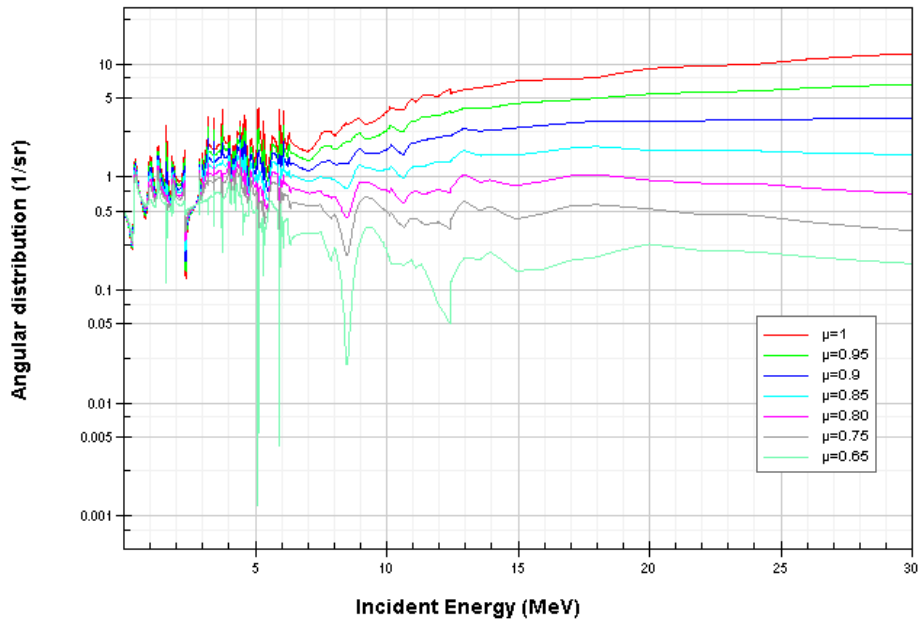
Figure 5 : Differential elastic scattering cross-section data for O-16

1.2.6 Neutron Detection

There are several types of devices or detectors that have been contrived for the observation of neutrons. In general, *neutron detectors* operate on the principle of detecting the energy that is released when a neutron interacts in the detector volume. The most common types of neutron detectors are gas-filled detectors. Usually, the fill gas is something with a high cross-section for neutron absorption (e.g. BF_3 or He^3).
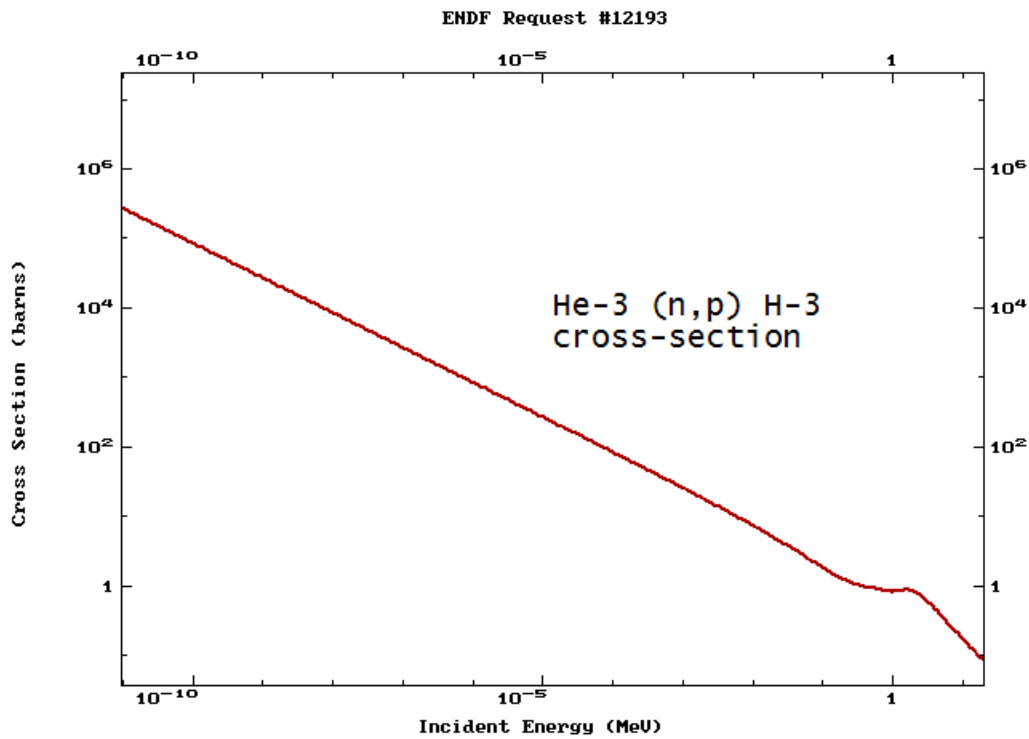
Figure 6 : He-3 (n,p) H-3 cross-section

11

In this study, only He^3 filled detectors were considered. The advantages of He^3 detectors are that the gas is chemically stable and high fill-pressures are attainable, which made them favorable for neutron well logging designs. He^3 detectors are typically cylindrical. They consist of a central anode, and the inner wall serves as the cathode. When neutrons interact with the nuclei of He-3 atoms inside the sealed volume, the most likely reaction is the (n,p) reaction:

$$He_2^3 + n_0^1 \rightarrow H_1^1 + H_1^3$$
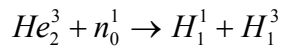
By conservation of momentum and mass-energy, the resultant proton can be shown to have 0.573 MeV and the triton to have 0.181 MeV of kinetic energy. This energy is expended by ionizing the helium atoms in the detector volume. An applied electric field drives the electrons, released in ionization, toward the central anode (Knoll). In a proportional counter, the electric field is strong enough that secondary ionizations occur as the electrons are accelerated toward the anode, and the arrival of all the electrons results in a voltage spike that is eventually registered as a 'count' after passing through some pulse shaping and amplification circuits. Compensated neutron logging detectors are typically operated as proportional counters.

Figure 6 makes it clear that the (n,p) reaction has a high cross-section. Even at neutron energies as high as 2 MeV, the cross-section is appreciable; which is a property that will be interesting when looking at detector responses to sources of different energies.

1.2.7 Neutron Transport

Neutron transport is the study of the behavior of neutron populations (Stacey). Equation 2 is the neutron transport equation adapted from Nuclear Reactor Physics for a source-driven system in a non-multiplying medium. The equation represents a balance of the neutron population in a phase space with the dimensions of position, direction, and neutron energy. In Equation 2 :

$\varphi(\bar{r}, \overline{\Omega}, E)$ represents the position ($\bar{r}$), direction ($\overline{\Omega}$), and energy (E) dependent neutron flux,

$\Sigma_t(\bar{r}, E)$ represents the total macroscopic cross-section (sum of scattering and

absorption) with position and energy dependence,

$\Sigma_s(\bar{r}, E' \to E, \mu_0)$ represents the differential scattering cross-section with dependence on

position, the cosine of the scattering angle ($\overline{\Omega}' \bullet \overline{\Omega} = \mu_0$), and the pre-scatter ($E'$)

and post-scatter neutron energies (E),

$S_{ex}(\bar{r}, \overline{\Omega}, E)$ represents the neutron source with direction, energy, and position

dependence.

$$\overline{\Omega} \bullet \nabla \varphi(\bar{r}, \overline{\Omega}, E) + \Sigma_t(\bar{r}, E)\varphi(\bar{r}, \overline{\Omega}, E)$$
$$= \int_0^\infty d\mu_0 \Sigma_s(\bar{r}, E' \to E, \mu_0)\varphi(\bar{r}, \overline{\Omega}', E') + S_{ex}(\bar{r}, \overline{\Omega}, E) \quad \textbf{Equation 2}$$

The left hand side of the neutron transport equation represents the rate at which neutrons are leaving the phase space either by streaming, scattering, or absorption.

The right hand side represents the rate at which neutrons enter the phase space by scattering from different directions and energies, and directly by the source.

One class of solution methods relies on discretization of the problem space, and attempts to numerically solve for the flux using cross-section data, source specifications, and geometry specifications as the input. The essential characteristic of this class of solution methods is *determinism,* as it relates to the behavior of neutrons. Such treatments have many applications, and they have reached a high degree of sophistication. Perhaps the greatest benefit of deterministic transport solution methods is that the neutron flux is calculated for every discrete phase-space element. Thus, deterministic methods can be said to provide a complete solution for the neutron flux. However, the completeness of solutions obtained by deterministic methods may be questioned due to inherent difficulties in estimating accuracy, precision, and uncertainty.

The Monte Carlo method is one of the most precise and robust ways to solve neutron transport problems. Its major drawback is computational expense. In the case of analog Monte Carlo, neutron behaviors are directly simulated as stochastic processes. Every event in the neutron lifetime is determined by the result of a random number generator and knowledge of the governing cumulative distribution functions. Data storage constraints complicate efforts to obtain a complete solution of the neutron flux, so certain events are recorded whenever they occur (e.g. neutron absorption in a detector volume). Often, the central limit theorem is applied to determine the statistical precision of the quantitative result. Given the complexity of the general problem space, millions, billions, or even greater numbers of neutron histories may need to be simulated to associate a desirably low variance with the calculated mean value.

2 Methods and Procedures

2.1 Monte Carlo Calculations

2.1.1 Geometry of the problem

The Monte Carlo calculations in this study were done using the MCNP5 (v1.4) code package (X-5). The geometry of the simulation is illustrated in Figure 7. The second view illustrates the eccentric positioning that is typical for wireline well logging tools. Both near and far detectors are He-3 filled proportional counters. The near detector fill pressure is 1.5 atm, and the far detector fill pressure is 4 atm. The near detector is smaller, and has a sleeve surrounding it that contains low-Z elements (such as carbon and hydrogen) to increase the count rate response by slowing down fast and intermediate neutrons. The moderation material (green) shown in Figure 7 is Titanium Hydride epoxy, and the shielding material (yellow) is B_4C, a strong thermal neutron absorber. The tool housing is made of stainless steel (Gardner).

2.1.2 Code options and flags

Here only the options and flags used are noted. For detailed information on the process, please refer to the MCNP5 manual, or Carter and Cashwell (Carter).
 The code was run in neutron transport only mode, since photons and electrons are not critical to the porosity log. No variance reduction techniques were used. Neutron path length multiplied by the He^3 (n,p) cross-section at the appropriate energy was tallied in the active detector volumes (or segments).

2.1.3 Nuclear data and cross-sections

All of the data used were provided in the MCNP5 distribution. No external data processing was necessary. ENDF-B6.0 data were used wherever unspecified. ENDF-B5.0 S(alpha,beta) tables were used for the hydrogen in the borehole water and the water filled porosity at 300K. It may be possible to improve the accuracy of the results by using S(alpha,beta) data more appropriate for the high temperature borehole environment. The values of these S(alpha,beta) data are very much dependent on temperature, and often affect the energy spectrum of thermal neutrons throughout the problem a great deal.
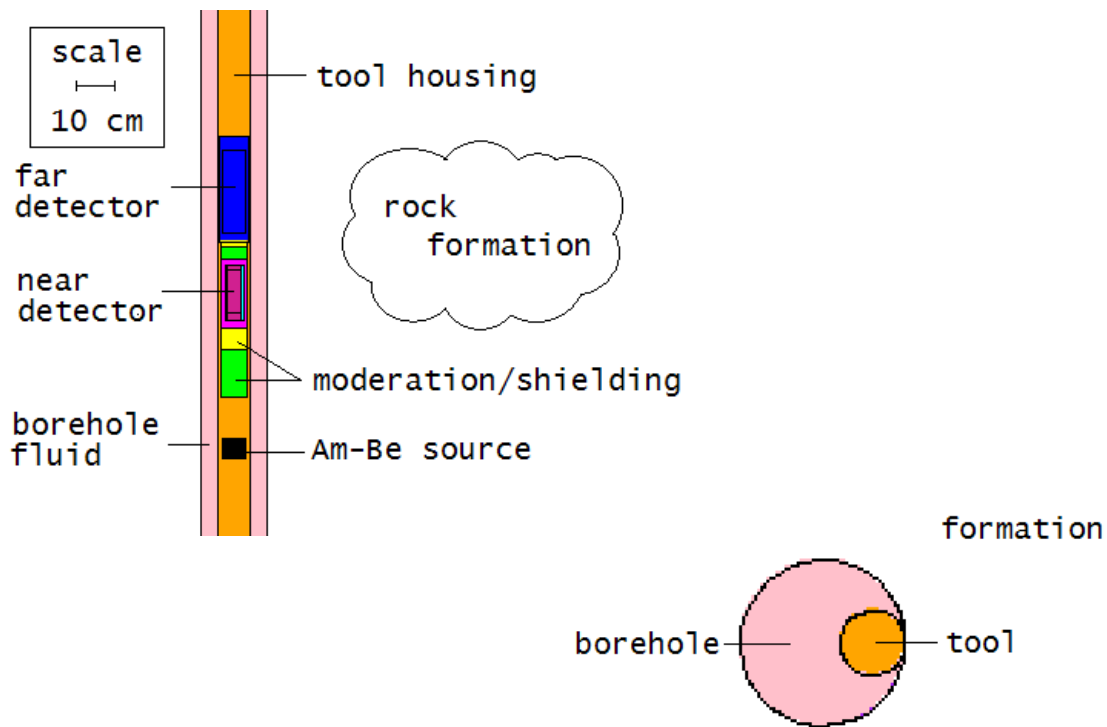
Figure 7 : Am-Be tool illustration

2.1.4 Computer system

All of the simulations were run on the Center for Engineering Applications of

Radioisotopes parallel computing cluster—dubbed "Spectral" (See

Figure 8.) The cluster consists of 49 nodes (as of 12/7/07), each equipped with an AMD

Athlon64 3400+ processor, 1 GB of RAM, and a 40 GB hard drive. Each node runs the

Slackware Linux (v11) distribution with a 64 bit Linux kernel (v. 2.6.21.5). The nodes are

interconnected via three unmanaged 100Mb/s Ethernet switches. The construction of the

cluster was part of the work involved in completing this thesis.

Figure 8 : Photograph of Computer System

2.2 Experiment Design

2.2.1 Understanding tool behavior

To understand the tool's behavior, the response to a number of variables needs to be observed. The primary independent variables of interest are the porosity of the formation and the neutron source energy distribution. A factorial experiment was carried out with 12 different porosities and 3 different neutron source energy distributions. Refer back to Figure 1 for the energy distributions, and the porosity values were 0, 1, 3, 5, 10, 15, 25, and 35% H_2O by volume. In each observation, 10^9 neutron histories were simulated. The neutron path length through each detector volume was tallied to estimate the neutron flux for each volume. The tally was separated into eight different energy bins, to examine how neutrons of different energies contribute to the count rate. The 'fm', tally multiplier, card of MCNP5 was used to multiply these neutron flux estimates by the (n,p) cross section of He^3, thereby arriving near an estimate of the detector count rate (X-5). The count rate was arrived at by multiplying the tally result by the volume of the detector and the source intensity. The count rate responses for each of the eight energy bins in both detectors provide 16 dependent variables for the analysis.

In contrast to the radioisotope sources, the accelerator source does not emit neutrons isotropically. The angular distribution for the accelerator source was assumed to be an exponential distribution described by:

$$p(\mu) = K * \exp(0.1 * \mu) \qquad \textbf{Equation 3}$$

Where $p(\mu)$ represents the value of the probability density function, and μ represents the cosine of the emission angle. K is just a normalization constant so that Equation 3 can be called a probability density function. The assumed distribution is approximate for an accelerator that produces deuterons in the tens of keV range. As the incident deuteron energy increases the neutrons distribution becomes more forward biased. The assumed distribution applies to the domain $-1 \leq \mu \leq 1$. $\mu = 1$ is oriented toward the detectors.

2.2.2 Optimizing detector position

To determine the effect of adjustments to detector position, simulations were performed with altered geometric input. In each of these simulations, the active volume for one type of detector (i.e. near or far) was extended over the entire region of interest and the neutron flux was estimated from path length tallies in segments approximately 5 cm long. The geometry for the far detector segmented tally experiments is illustrated in Figure 9.

2.2.3 Depth of Penetration

A series of 21 simulated experiments were conducted to determine the differences in depth of penetration of the three sources. The new independent variable for these experiments was the radius of the right-circular cylindrical rock formation. The counting yields for the near and far detectors were observed for each of the sources and for the following rock formation radii: 30 cm, 35 cm, 40 cm, 45 cm, 50 cm, 55 cm, and 60 cm. The porosity was held constant at 10%. The depth of penetration is related to the radius at which the counting yields reach 95% of the counting yields obtained in the experiments described under section 2.2.1 (where the formation radius was effectively infinite.)

19
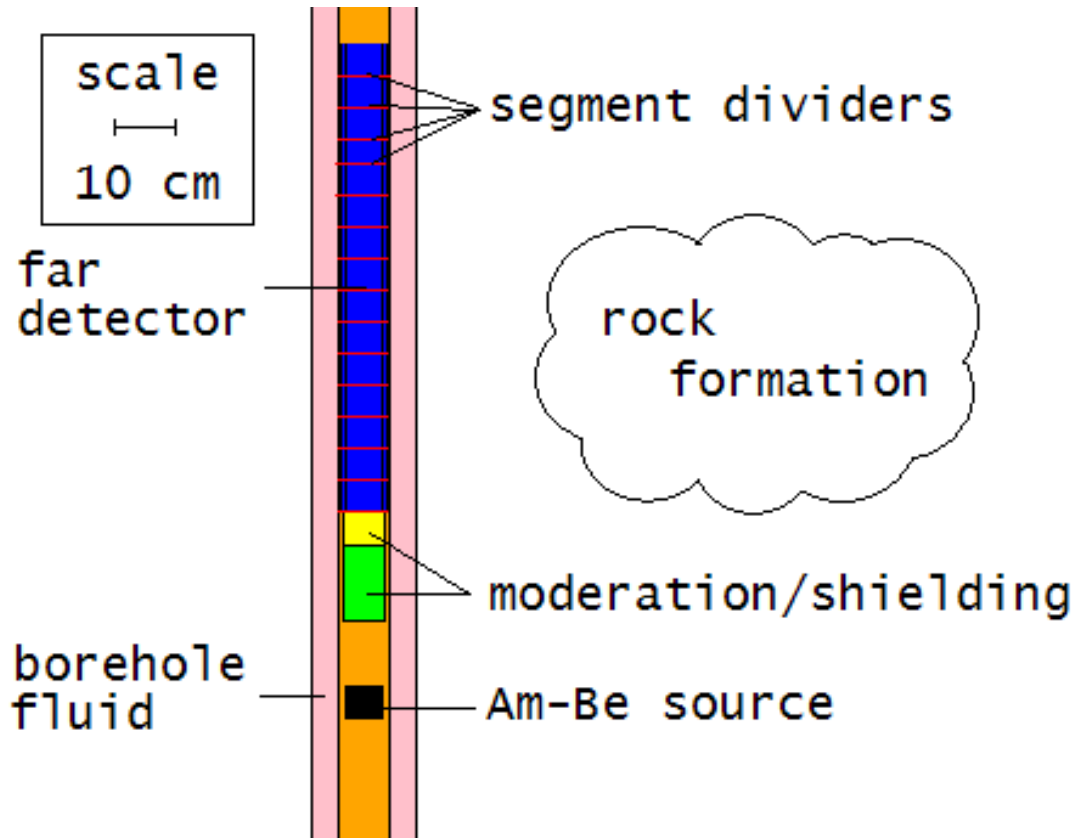
Figure 9 : Segmented tally geometry

3 Simulation Results

Figure 10 through Figure 12 illustrate the responses of both near and far detectors for all three source types. MCNP5 automatically scales tally results by the total number of histories. The counting yields presented were obtained by multiplying the tally mean estimates by the volume of the active detector region. To get the predicted count rate, one would multiply these counting yields by the source intensity.

Estimates of the standard deviation for each of the mean reaction rate densities were obtained automatically by MCNP5, which uses the standard estimator for variance. The estimate of standard deviation divided by the mean is called the *relative error.* The relative error was greatest for the californium source simulations, and smallest for the accelerator source simulations. Relative error also tended to increase for the simulations with high porosity. Many estimates of the relative error were as low as 0.1%, but the worst case (i.e. far detector, californium source, at 35% porosity) relative error was 2.32%.

Figure 13 and Figure 14 illustrate the near-to-far detector response ratios for each source across the range of porosities. The former is a semi-log plot, and the latter is a linear plot of the same information. The near-to-far ratio is the signal of choice in neutron porosity logging practice. The propagation of the Monte Carlo calculation errors resulted in relative errors between 0.2% and 2.36% for the ratios.
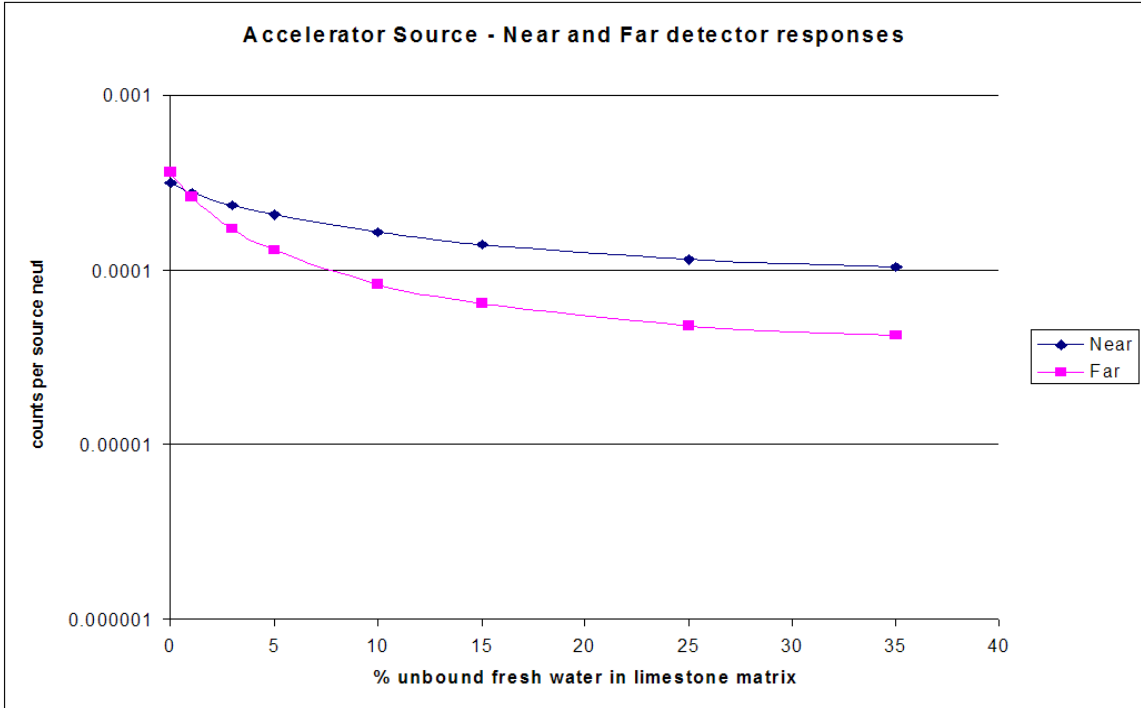
Figure 10 : Near and Far detector responses, Accelerator source
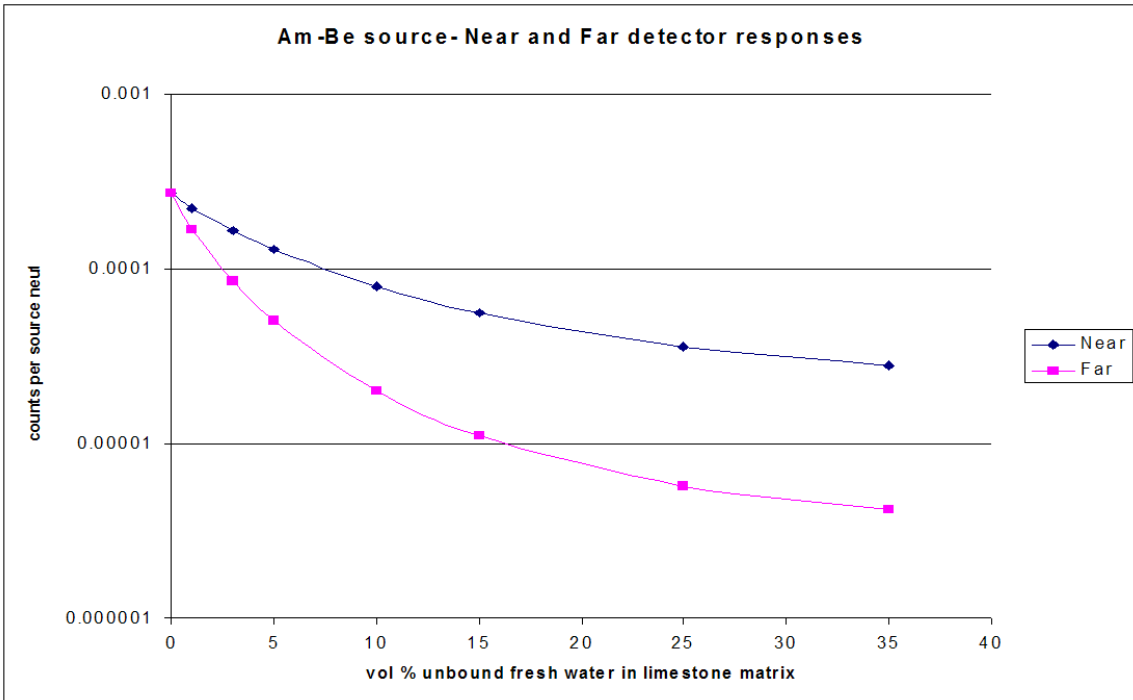
Figure 11: Near and Far detector responses, Am-Be source

22
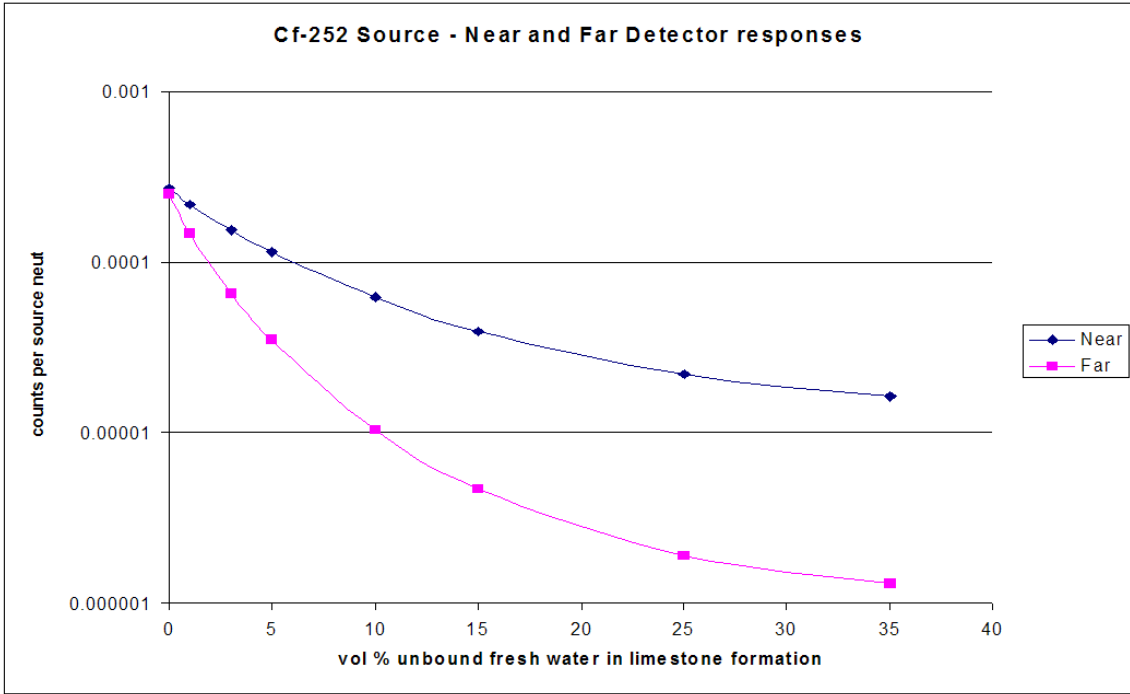
Figure 12: Near and Far detector responses, Californium source
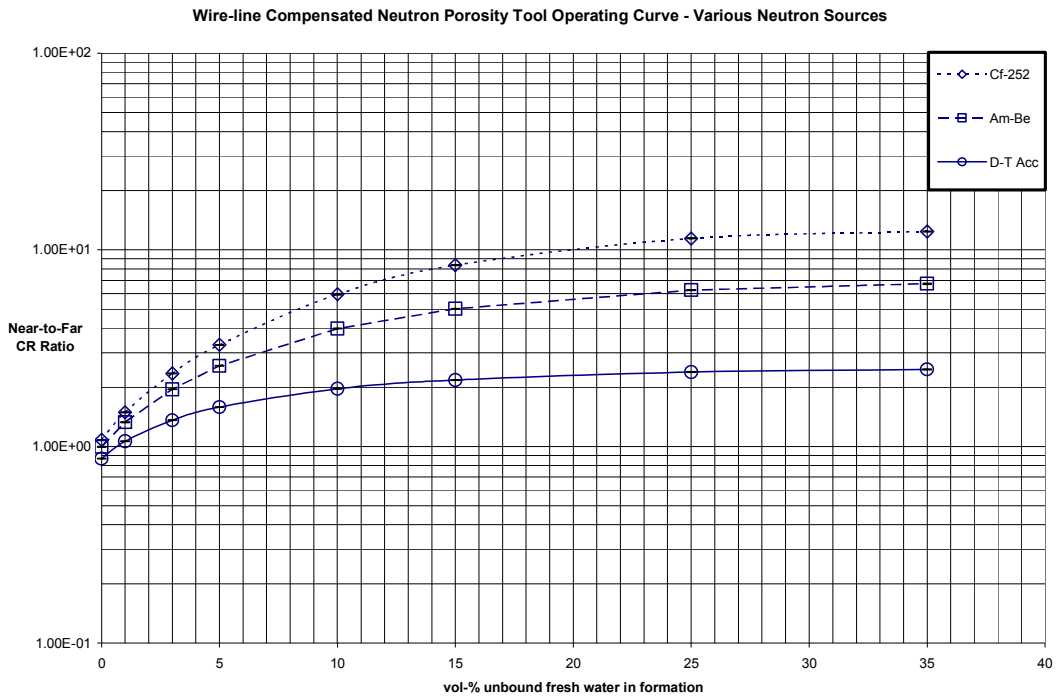
Figure 13: Near-to-Far Count Rate Ratio Results, Semi-Log
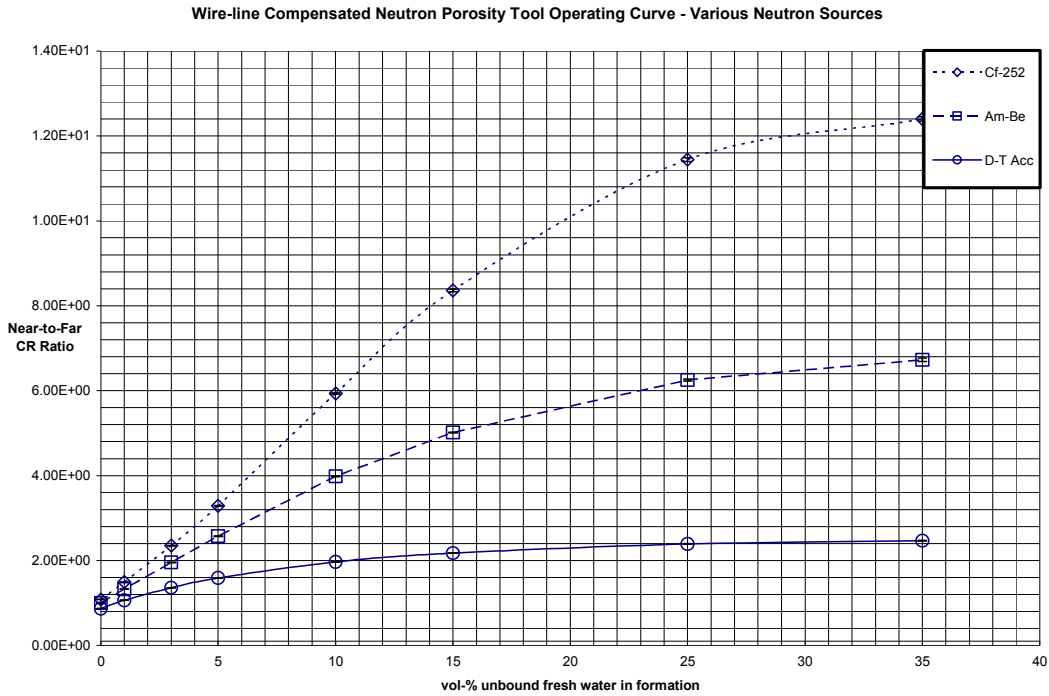
Figure 14: Near-to-Far Count Rate Ratio Results, Linear

For each source, detector, and porosity, Table 1 through

Table 6 shows the fraction of the total count rate that comes from each neutron

energy group. For the far detector, californium source, and high porosity, some of the energy

group yield estimates were subject to as much as 7% relative error. The minimum relative

error for any of these energy group estimates is 0.5%. Although the tabulated percentages

are technically derived quantities (energy group response/total response), after propagation

the relative error is completely dominated by the energy group relative error.

Figure 15 through Figure 20 show all of the un-normalized energy group

contributions to total count yield. The relative error estimates for the data in these figures are

also in the 0.5% to 7% range.

24

Table 1: AmBe Source, Near Detector Response Breakdown by Neutron Energy

Porosities	Energy Ranges, MeV									
	$0-10^{-8}$	$10^{-8}-10^{-7}$	$10^{-7}-10^{-6}$	$10^{-6}-10^{-5}$	$10^{-5}-10^{-4}$	$10^{-4}-10^{-3}$	$10^{-3}-10^{-2}$	$10^{-2}-10^{-1}$	$10^{-1}-10^{0}$	10.0-14.1
0	7.39%	72.78%	15.48%	2.99%	0.95%	0.29%	0.08%	0.02%	0.01%	0.00%
1	7.56%	74.56%	14.30%	2.47%	0.78%	0.24%	0.07%	0.02%	0.01%	0.01%
3	7.73%	76.25%	13.13%	1.99%	0.62%	0.19%	0.06%	0.02%	0.01%	0.01%
5	7.74%	77.12%	12.54%	1.77%	0.56%	0.18%	0.05%	0.02%	0.01%	0.01%
10	7.83%	77.69%	12.05%	1.63%	0.53%	0.17%	0.06%	0.02%	0.01%	0.01%
15	7.78%	77.59%	12.10%	1.69%	0.55%	0.19%	0.06%	0.02%	0.01%	0.01%
25	7.74%	77.36%	12.20%	1.78%	0.60%	0.21%	0.07%	0.02%	0.01%	0.01%
35	7.82%	76.96%	12.40%	1.86%	0.63%	0.22%	0.07%	0.02%	0.01%	0.01%

Table 2: AmBe Source, Far Detector Response Breakdown by Neutron Energy

Porosities	Energy Ranges, MeV									
	$0,10^{-8}$	$10^{-8}, 10^{-7}$	$10^{-7}, 10^{-6}$	$10^{-6}, 10^{-5}$	$10^{-5},10^{-4}$	$10^{-4}, 10^{-3}$	$10^{-3},10^{-2}$	$10^{-2},10^{-1}$	$10^{-1},10^{0}$	10.0-14.1
0	1.55%	62.86%	25.24%	7.02%	2.40%	0.70%	0.18%	0.04%	0.01%	0.01%
1	1.71%	68.25%	22.27%	5.25%	1.77%	0.54%	0.15%	0.04%	0.02%	0.01%
3	1.83%	72.08%	19.95%	4.05%	1.42%	0.45%	0.13%	0.04%	0.02%	0.02%
5	1.87%	72.78%	19.49%	3.78%	1.40%	0.46%	0.14%	0.04%	0.02%	0.02%
10	1.80%	72.06%	19.84%	3.92%	1.56%	0.52%	0.17%	0.05%	0.03%	0.04%
15	1.88%	70.78%	20.24%	4.40%	1.72%	0.63%	0.20%	0.06%	0.04%	0.05%
25	1.72%	70.31%	19.84%	4.89%	2.07%	0.73%	0.24%	0.08%	0.05%	0.07%
35	1.83%	69.62%	20.44%	4.88%	2.01%	0.75%	0.25%	0.08%	0.06%	0.08%

Table 3: Accelerator Source, Near Detector Response Breakdown by Neutron Energy

Porosities	Energy Ranges, MeV									
	$0,10^{-8}$	$10^{-8}, 10^{-7}$	$10^{-7}, 10^{-6}$	$10^{-6}, 10^{-5}$	$10^{-5},10^{-4}$	$10^{-4}, 10^{-3}$	$10^{-3},10^{-2}$	$10^{-2},10^{-1}$	$10^{-1},10^{0}$	10.0-14.1
0	7.45%	72.75%	15.32%	3.01%	1.00%	0.32%	0.10%	0.03%	0.01%	0.01%
1	7.55%	73.94%	14.56%	2.67%	0.87%	0.28%	0.09%	0.03%	0.01%	0.01%
3	7.66%	75.23%	13.68%	2.30%	0.75%	0.24%	0.08%	0.02%	0.01%	0.01%
5	7.77%	75.73%	13.27%	2.16%	0.71%	0.23%	0.07%	0.02%	0.01%	0.02%
10	7.71%	76.35%	12.89%	2.02%	0.68%	0.22%	0.07%	0.02%	0.02%	0.02%
15	7.81%	76.35%	12.81%	2.00%	0.67%	0.23%	0.07%	0.02%	0.02%	0.02%
25	7.77%	76.44%	12.76%	1.98%	0.68%	0.23%	0.08%	0.02%	0.02%	0.02%
35	7.80%	76.42%	12.74%	1.99%	0.67%	0.23%	0.08%	0.03%	0.02%	0.02%

Figure 23 and Figure 24 contain the results of the depth of penetration experiments. The plotted data are the ratios of the counting yields observed in the penetration experiments (section 2.2.3) to those corresponding yields obtained in the experiments described in section 2.2.1.

The noticeable blip in the Am-Be data at 50 cm radius is an artifact due to the lesser number of histories that were completed for that simulation. The inconsistency is the result of premature simulation termination due to another user's interference with the computer's operation.

Table 4: Accelerator Source, Far Detector Response Breakdown by Neutron Energy

Porosities	Energy Ranges, MeV									
	$0,10^{-8}$	$10^{-8}, 10^{-7}$	$10^{-7}, 10^{-6}$	$10^{-6}, 10^{-5}$	$10^{-5},10^{-4}$	$10^{-4}, 10^{-3}$	$10^{-3},10^{-2}$	$10^{-2},10^{-1}$	$10^{-1},10^{0}$	10.0-14.1
0	1.55%	62.07%	25.09%	7.41%	2.68%	0.85%	0.24%	0.06%	0.03%	0.02%
1	1.65%	65.95%	23.04%	6.10%	2.21%	0.72%	0.21%	0.06%	0.03%	0.03%
3	1.74%	68.59%	21.53%	5.23%	1.93%	0.65%	0.20%	0.06%	0.04%	0.04%
5	1.74%	69.44%	21.01%	4.94%	1.87%	0.65%	0.21%	0.06%	0.04%	0.05%
10	1.75%	69.60%	20.70%	4.96%	1.91%	0.68%	0.22%	0.07%	0.05%	0.07%
15	1.70%	69.20%	20.98%	4.98%	2.00%	0.71%	0.23%	0.07%	0.05%	0.08%
25	1.65%	68.80%	21.07%	5.22%	2.04%	0.75%	0.25%	0.08%	0.05%	0.09%
35	1.66%	68.86%	21.02%	5.16%	2.06%	0.75%	0.25%	0.08%	0.06%	0.10%

Table 5: Californium Source, Near Detector Response Breakdown by Neutron Energy

Porosities	Energy Ranges, MeV									
	$0,10^{-8}$	$10^{-8}, 10^{-7}$	$10^{-7}, 10^{-6}$	$10^{-6}, 10^{-5}$	$10^{-5},10^{-4}$	$10^{-4}, 10^{-3}$	$10^{-3},10^{-2}$	$10^{-2},10^{-1}$	$10^{-1},10^{0}$	10.0-14.1
0	7.39%	72.76%	15.56%	2.98%	0.94%	0.28%	0.08%	0.02%	0.01%	0.00%
1	7.62%	74.60%	14.32%	2.43%	0.74%	0.22%	0.06%	0.02%	0.01%	0.00%
3	7.77%	76.72%	12.87%	1.85%	0.56%	0.17%	0.05%	0.01%	0.01%	0.00%
5	7.84%	77.72%	12.13%	1.59%	0.49%	0.15%	0.04%	0.01%	0.01%	0.00%
10	7.80%	78.41%	11.66%	1.45%	0.45%	0.15%	0.05%	0.01%	0.01%	0.00%
15	7.89%	78.16%	11.69%	1.52%	0.49%	0.16%	0.05%	0.02%	0.01%	0.01%
25	7.73%	77.68%	12.11%	1.61%	0.56%	0.20%	0.06%	0.02%	0.01%	0.01%
35	7.79%	77.17%	12.30%	1.78%	0.63%	0.21%	0.07%	0.02%	0.01%	0.01%

Table 6: Californium Source, Far Detector Response Breakdown by Neutron Energy

| Porosities	Energy Ranges, MeV									
	$0,10^{-8}$	$10^{-8}, 10^{-7}$	$10^{-7}, 10^{-6}$	$10^{-6}, 10^{-5}$	$10^{-5},10^{-4}$	$10^{-4}, 10^{-3}$	$10^{-3},10^{-2}$	$10^{-2},10^{-1}$	$10^{-1},10^{0}$	10.0-14.1
0	1.55%	63.30%	25.15%	6.90%	2.29%	0.63%	0.15%	0.03%	0.01%	0.00%
1	1.74%	69.17%	22.10%	4.83%	1.56%	0.45%	0.11%	0.03%	0.01%	0.01%
3	1.86%	74.15%	19.01%	3.35%	1.14%	0.35%	0.10%	0.03%	0.01%	0.01%
5	1.85%	75.26%	18.37%	2.96%	1.06%	0.34%	0.10%	0.03%	0.02%	0.01%
10	1.91%	74.16%	18.59%	3.38%	1.27%	0.45%	0.14%	0.04%	0.03%	0.02%
15	1.92%	72.03%	19.39%	4.17%	1.56%	0.62%	0.17%	0.06%	0.04%	0.04%
25	1.92%	69.04%	20.62%	5.09%	2.08%	0.82%	0.24%	0.08%	0.05%	0.06%
35	1.39%	68.03%	21.92%	5.28%	2.09%	0.83%	0.25%	0.09%	0.06%	0.08%
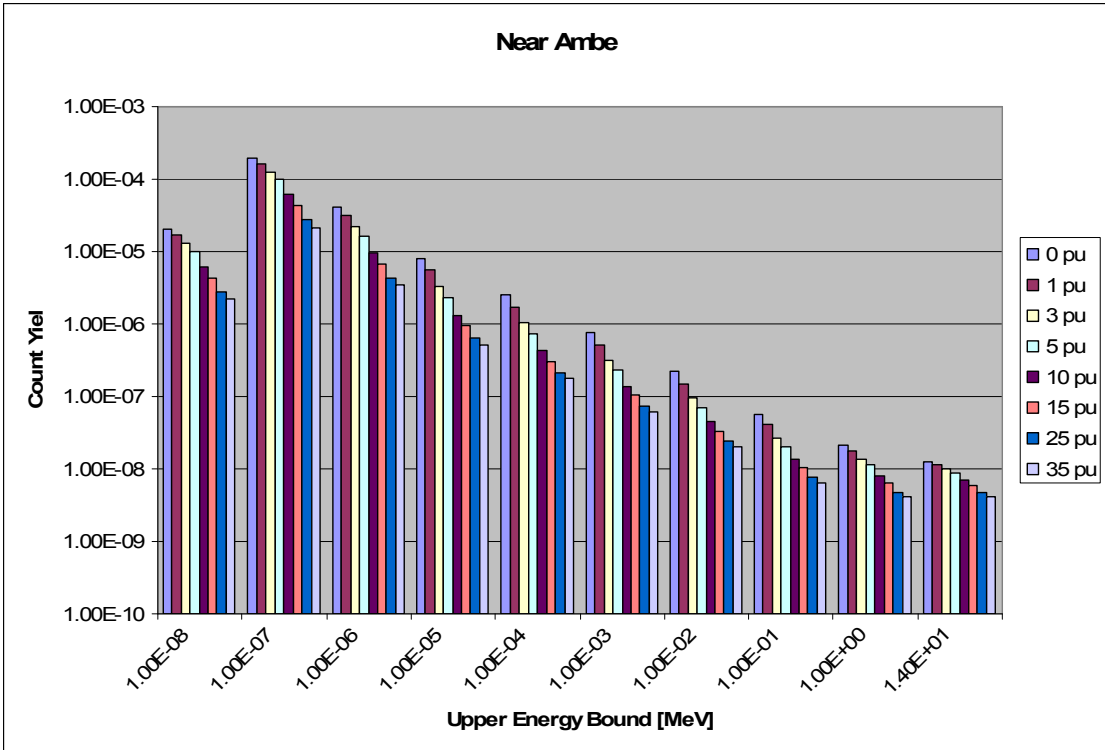
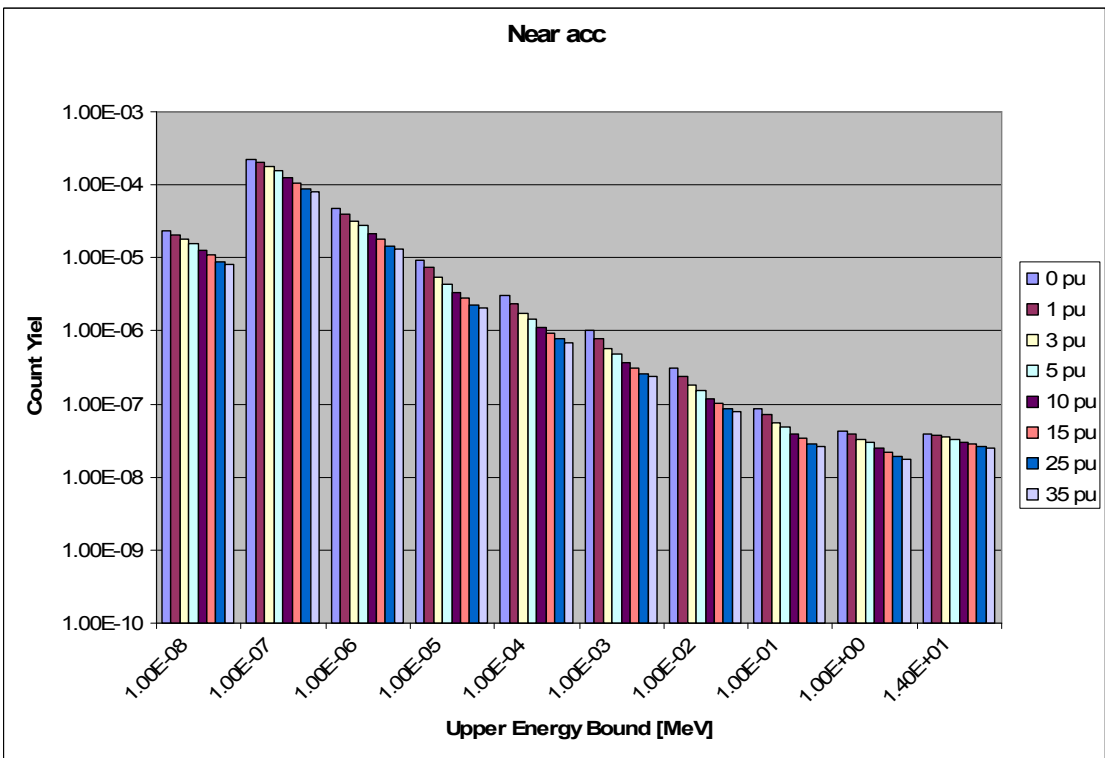**Figure 15: Energy-dependent responses, Near Am-Be**

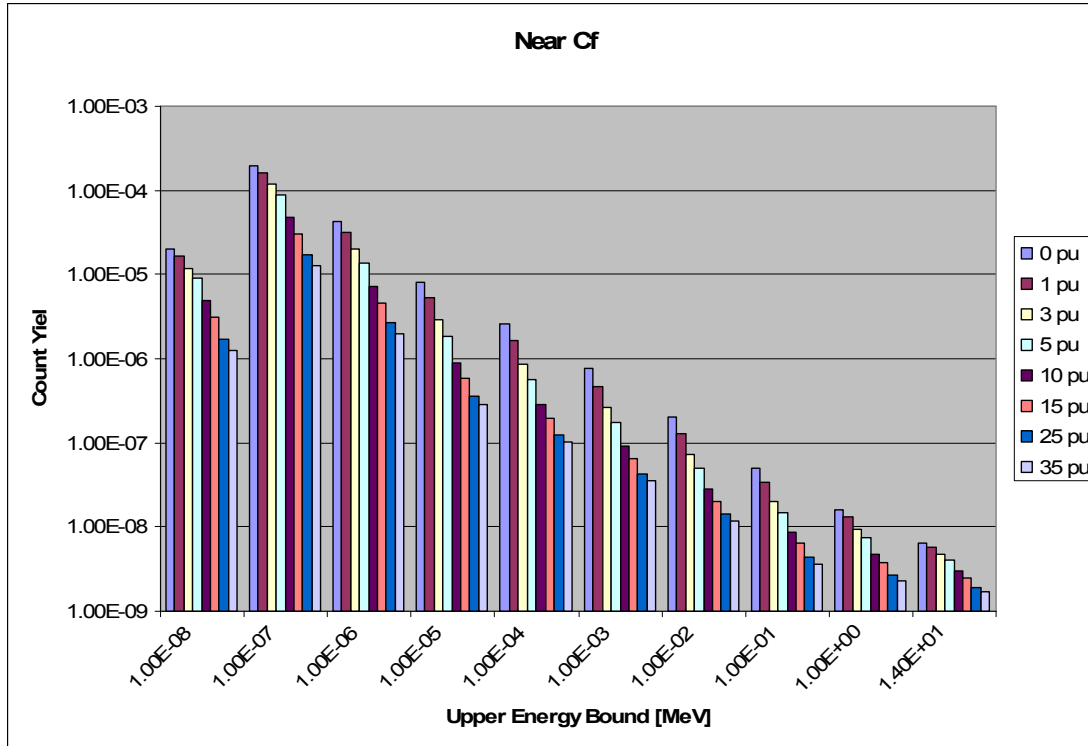**Figure 16: Energy-dependent responses, Near Accelerator**

27

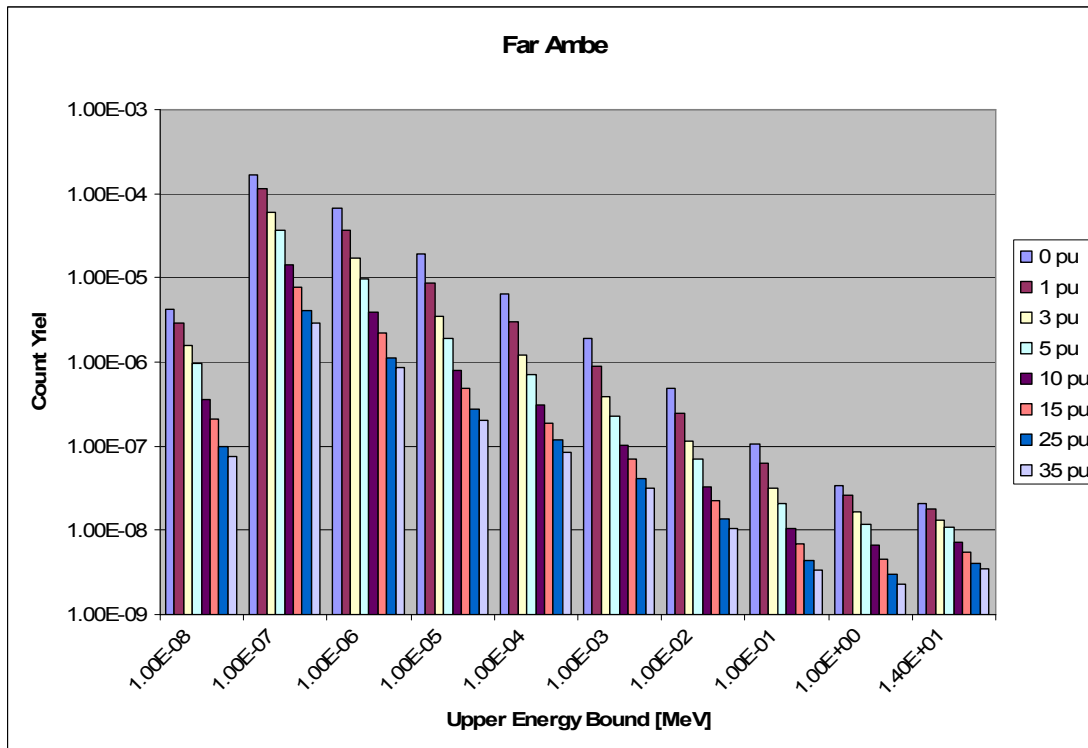**Figure 17: Energy-dependent responses, Near Californium**

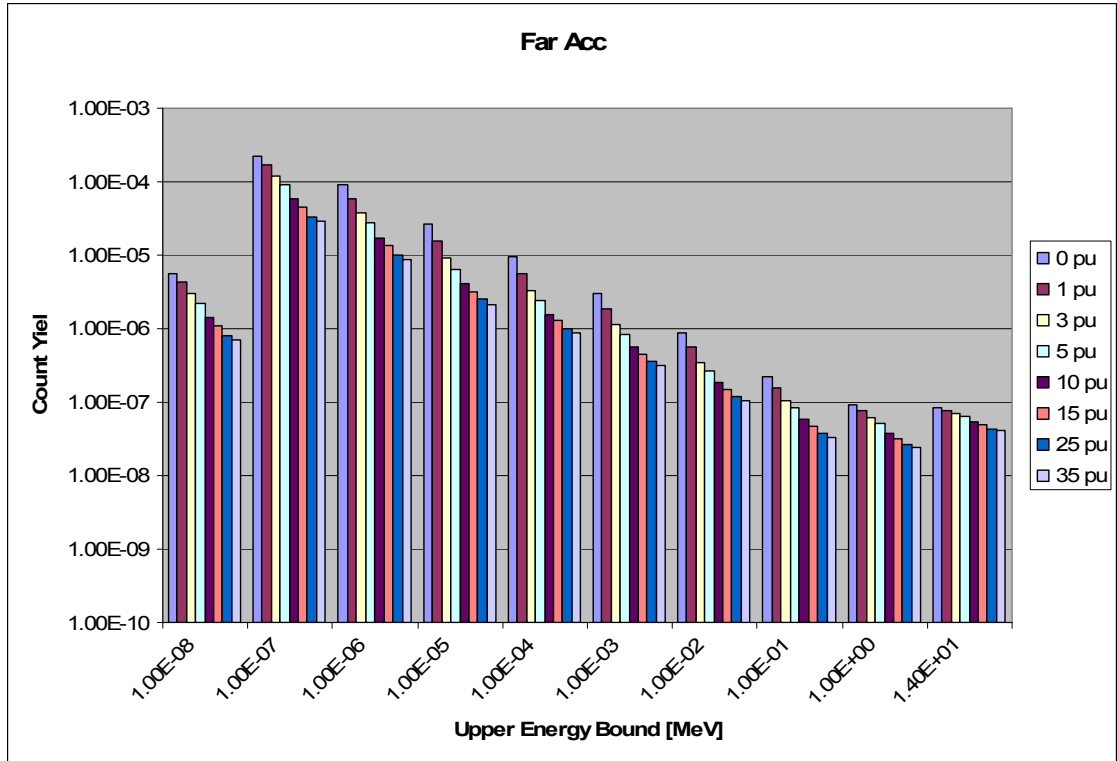**Figure 18: Energy-dependent responses, Far Am-Be**

28

Figure 19: Energy-dependent responses, Far Accelerator
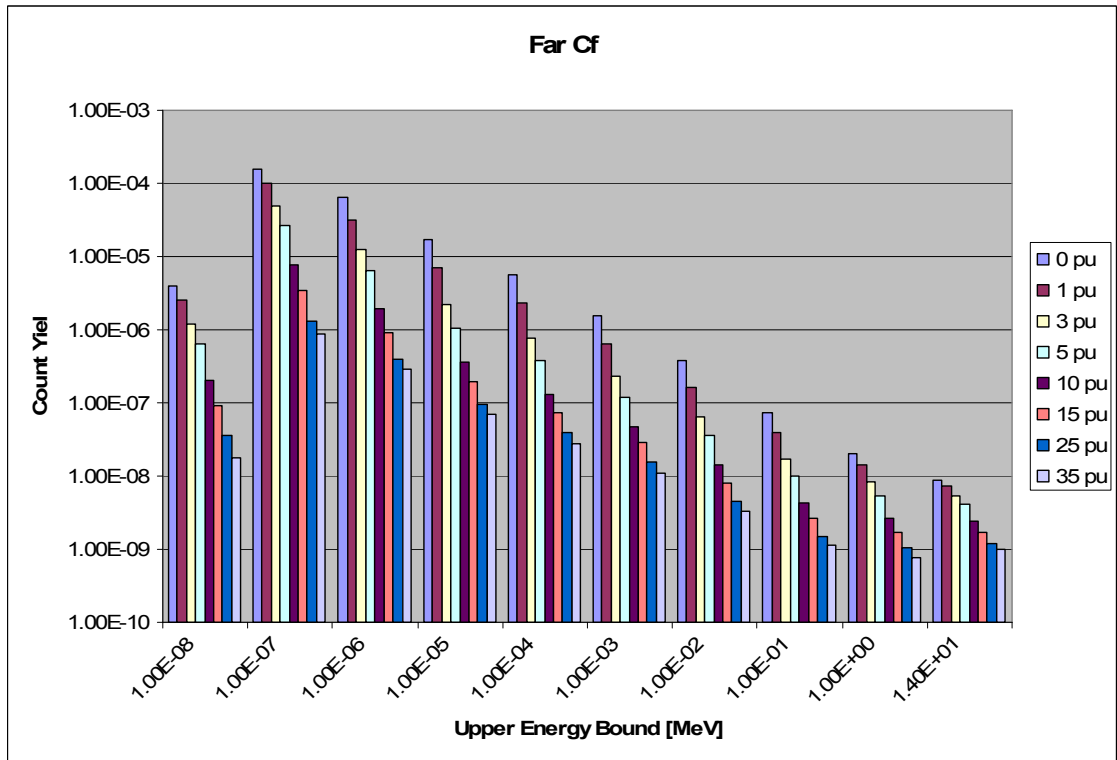

Figure 20: Energy Dependent Responses, Far Californium

29

Far Detector Reaction Rate Density - D-T Accelerator in Limestone
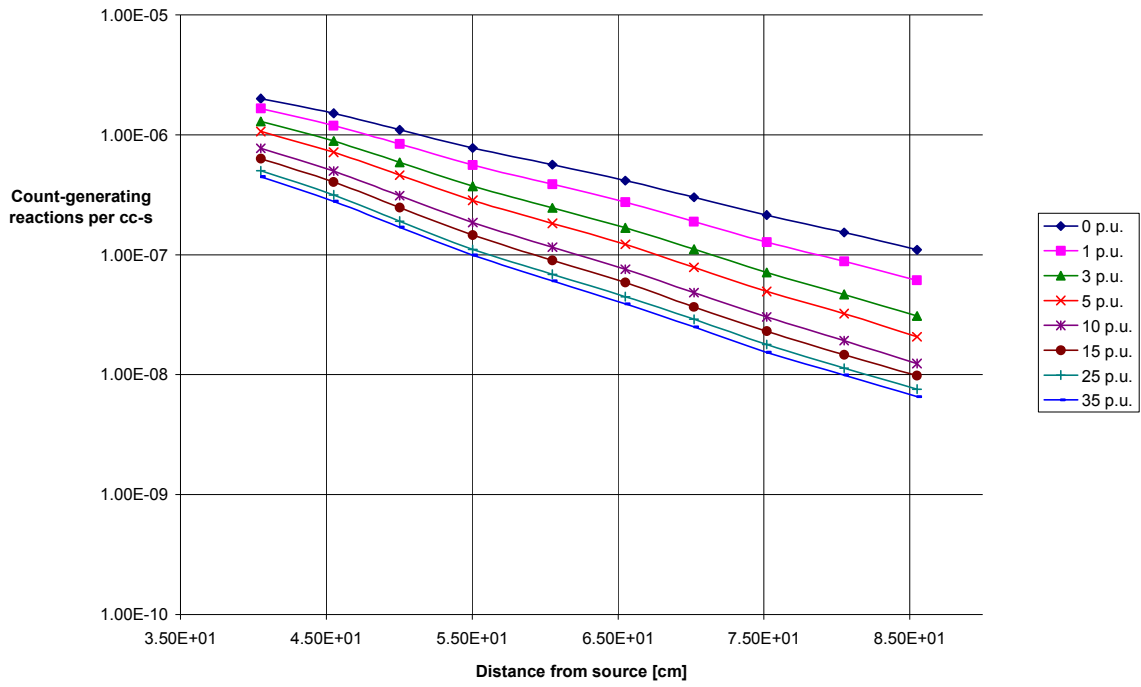

Figure 21: Far Detector Segmented Tally Results, Accelerator Source

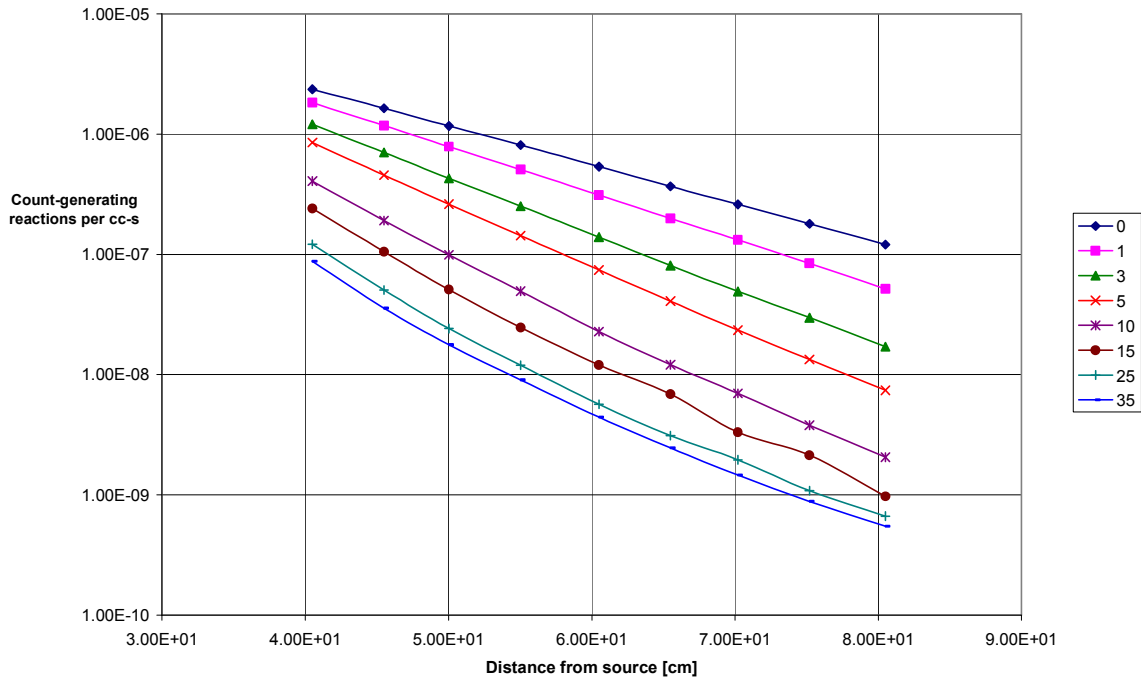**Far Detector Reaction Rate Density - Cf-252 in Limestone**

Figure 22: Far Detector Segmented Tally Results, Cf-252 Source
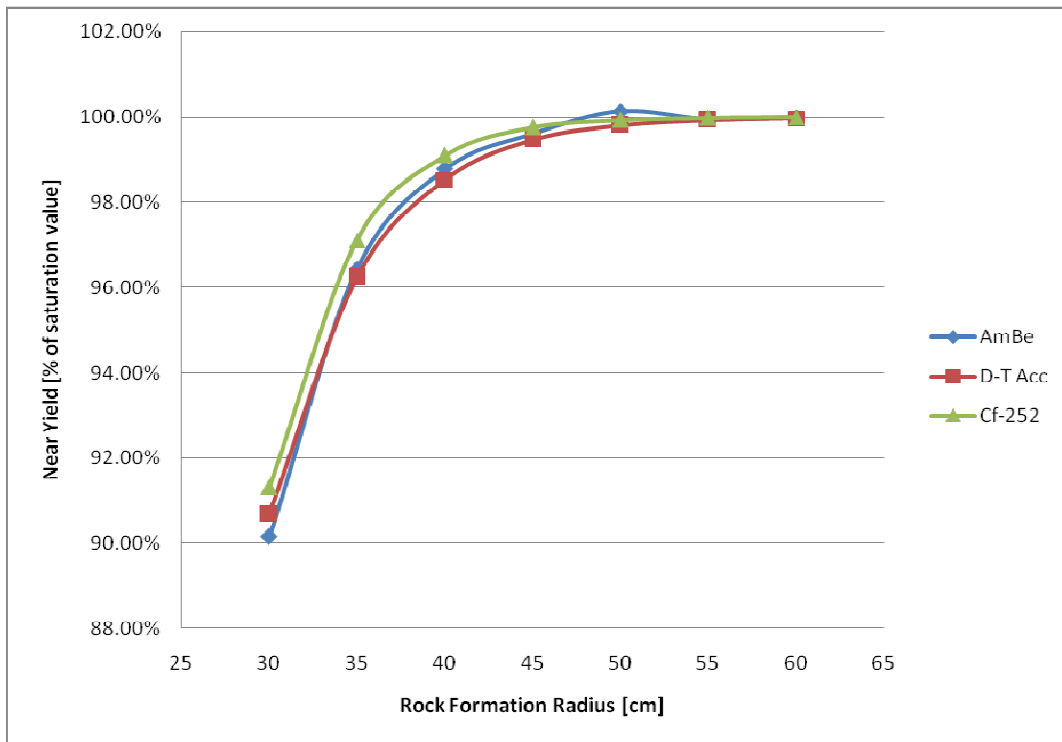
Figure 23: Results of Penetration Experiments, Near Detector
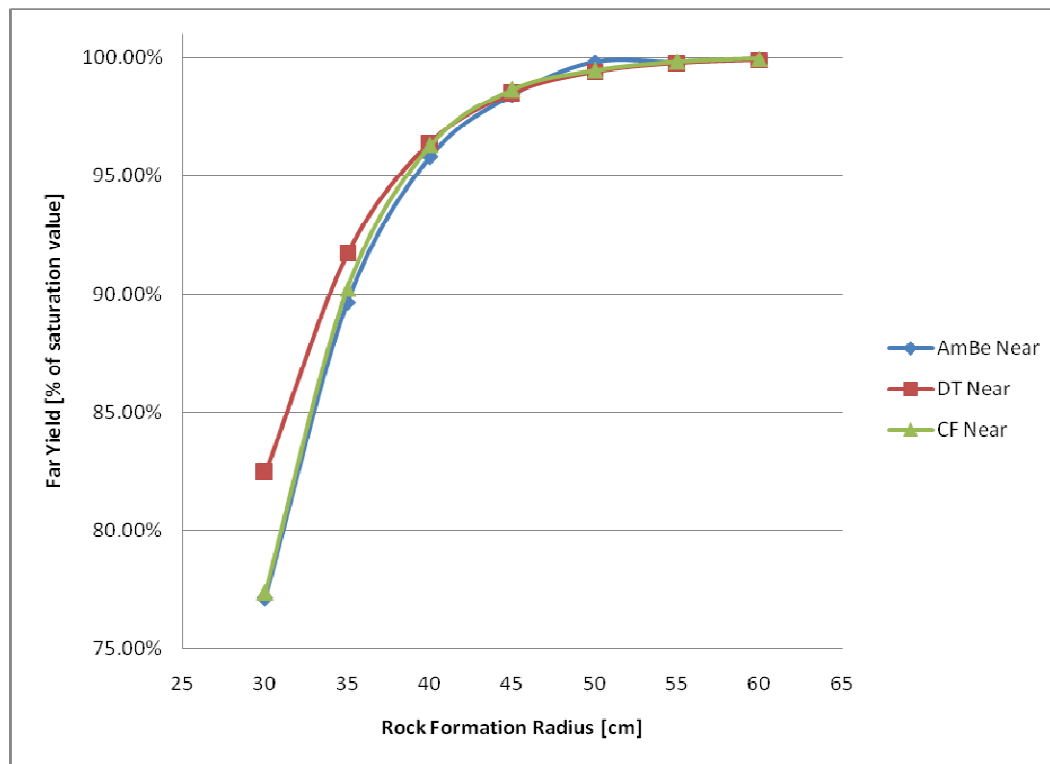
Figure 24: Results of Penetration Experiments, Far Detector

31

4 Discussion and Conclusions

It is too tempting to look for the pleasingly simple answer; that neutron porosity logging is technically feasible with the reference design in conjunction with any of the three neutron sources. Fortunately, the data do seem to suggest such simplicity. There are also some interesting tradeoffs that may provide design spaces with potential for further optimization.

The precision of the reference design is considered acceptable for interpretation *a priori*. It is used to compare against the precision obtainable with the other sources—See Figure 25.

Figure 25: Reference for acceptable precision

4.1 The californium replacement

The near-to-far ratio response obtained with the californium source appears to be quite a bit more sensitive than that obtained with the Am-Be source. However, as was noted in a previous st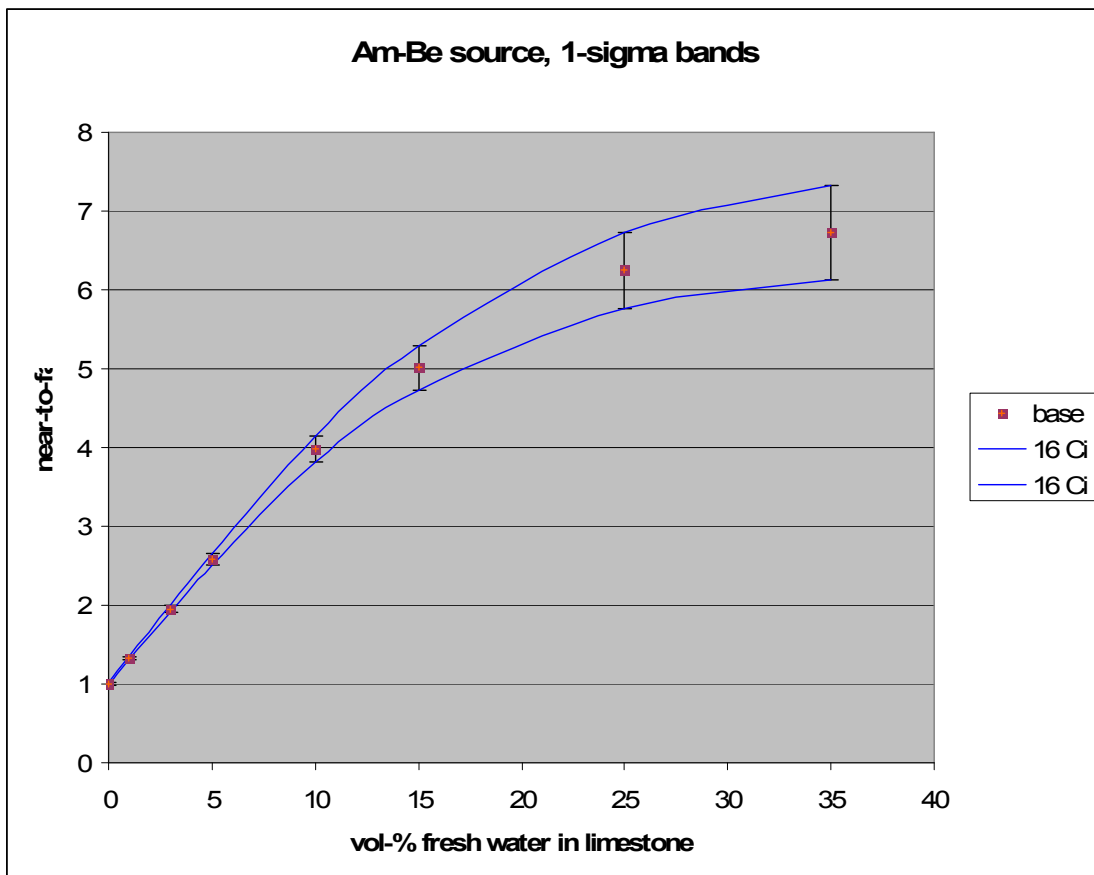udy, the lower counting yield will result in more error from counting statistics. To quantify this trade-off, it is necessary to introduce some information on the source intensities. The source intensity data in Table 7 was obtained by hand calculations involving basic nuclear data, except for the accelerator source data which came from the sales literature.

Table 7: Source intensities

	Source Intensities			
	intensity	intensity units	reference activity	reference intensity
Am-Be	2.19E+06	n/Ci-s	16 Ci	3.50E+07 n/s
Cf-252	4.30E+09	n/Ci-s	0.1 Ci	4.30E+08 n/s
D-T Acc.	1.00E+08	n/s	n/a	1.00E+08 n/s

In Figure 12 for the californium source, the yield ranges from $\sim 3*10^{-4}$ to $\sim 10^{-6}$. At the reference activity, these yields correspond to count rates of 11,700 cps to 563 cps. Since well-logging tools move quickly, the counting time is assumed to be 1 second. Applying Poisson statistics for count rate uncertainty (as in Equation 4) is standard practice.

$$\sigma = \frac{\sqrt{N}}{t} \qquad\qquad \textbf{Equation 4}$$

Where σ is the count-rate 'uncertainty' and N is the total counts observed in the counting interval t. The relative error from counting statistics in the single detector count rates is then increased by 0.3%-4.2% at the reference intensity. The near-to-far ratio then has a maximum relative error of 4.4%.

The example calculation at the reference activity would provide a nice response for well-logging. However, 0.100 Ci is a fairly large amount of californium-252 (0.187 mg). If instead the source were only 0.050 Ci (0.093 mg), the relative error in the ratio would get as high as 6.2%. At 0.025 Ci (0.047 mg), the relative error goes up to 8.78%.

Even at 0.025 Ci, no obvious problems with log interpretation arise. In the cases presented in the previous paragraph, the reduced yield that is a consequence of the low-energy neutron spectrum of Cf-252 is compensated for by the increased neutron source intensity. A Cf-252 source may be useful for porosity logs all the way down to 5 mCi (0.001 mg)—See Figure 26.
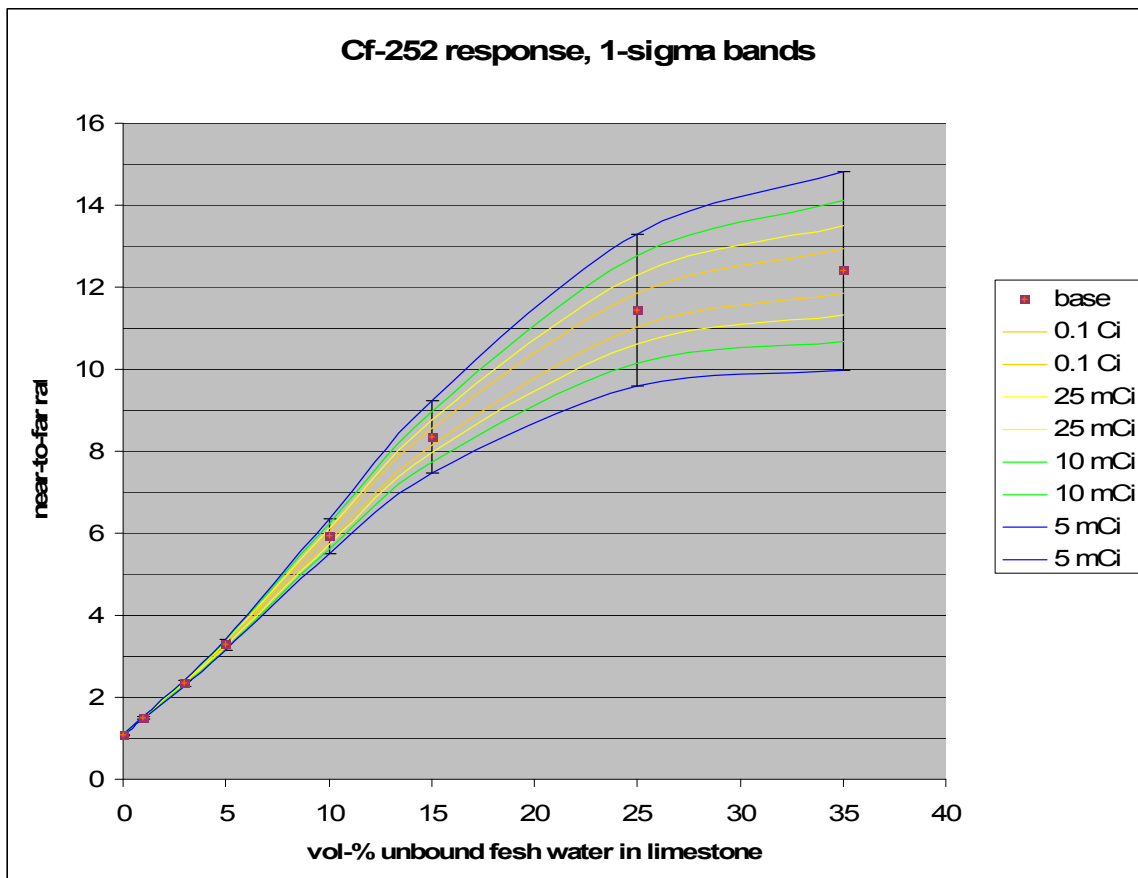

Figure 26: Porosity log precision declining with source activity, 1 sec counting interval

4.2 The accelerator replacement

Unlike in the californium source case, the accelerator source case has high yield. Like the californium source, it also has high source intensity. The accelerator source ratio response appears to be less sensitive than the Am-Be source ratio response. However, the low sensitivity is mitigated by much higher count rates; which will reduce the uncertainty due to counting statistics. The yields range from $3*10^{-4}$ to $4*10^{-5}$. Given the source intensity in Table 7, count rates are between 30,000 cps and 4,000 cps. So, the maximum near-to-far ratio relative error is 3%. Lower operating intensities could extend source lifetime and decrease maintenance costs—See Figure 27.

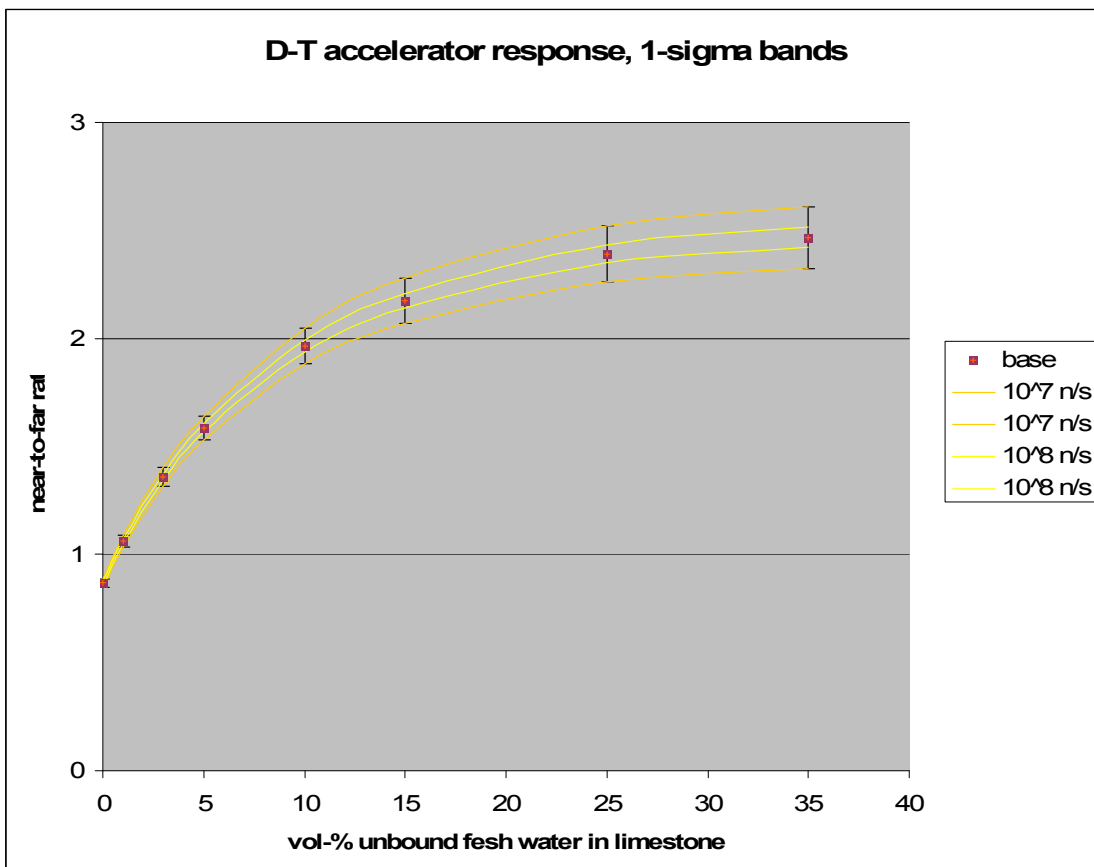**D-T accelerator response, 1-sigma bands**

legend:
- base
- 10^7 n/s
- 10^7 n/s
- 10^8 n/s
- 10^8 n/s

y-axis: near-to-far rat

x-axis: vol-% unbound fesh water in limestone

Figure 27: (D-T Accelerator) Porosity log precision okay at 10^7 n/s ?

4.3 General trends in the energy-dependent response

These results can provide further insight into the microscopic physical processes that contribute to the observed well log phenomena.

4.4 Detector Spacing

A consensus does not yet exist on the experimental method used to examine the effect of detector spacing. There are some concerns over the absorbing effect of He^3 as well as the effect of the missing section of moderation/shielding for the far detector cases. Until the method can be defended and trusted more readily, the analysis of its results will not go too deep.

The results that were obtained showed that the log-transformed reaction rate density vs. distance from the source for the far detector exhibited a linear correlation coefficient of > -0.99. For both alternate sources and for all porosities, this exponential trend was observed. For accelerator neutron source porosity well logs, it does appear that longer spacing of the far detector has potential to improve the near-to-far ratio sensitivity to porosity, but no conclusion can be drawn about whether this improvement justifies the decreased count-rate that a longer spacing would induce.

The following is in regard to the Cf-252 cases. It does appear clear that reducing the spacing of the far detector could improve count rate in the far detector, and that this would justify the reduction in sensitivity of the ratio response to porosity. However, note that reducing the spacing would require other significant changes to the tightly packaged design.

4.5 Depth of Penetration

More variation in the depth sensitivity of the different sources was expected. Most surprising was that the D-T source appears to exhibit the least sensitivity to depth as measured by the far detector counting yield (Figure 24.) The smaller cross-sections for high energy neutrons are a compelling reason to expect deeper penetration from the highest-energy neutron source.

4.5.1 The Borehole Background Theory

However, the seeming contradiction (that we see in Figure 24) of reason, may in fact be a confirmation in disguise. One may assume that neutrons scattering through the borehole fluid, water in these experiments, contribute some background noise to the counting rate in either detector. The counts from these neutrons are considered background, because they do not provide any information about the rock formation. The 'borehole background' count is not sensitive to the radius of the rock formation.

If the borehole background makes up a greater fraction of the total saturation yield for the D-T accelerator, then the penetration depth as expressed in Figure 24 would tend to be understated in comparison with the other sources. For example, if one were to run experiments with no rock formation but only the borehole fluid, the D-T source would register a higher percentage of its saturation yield than the other sources would.

The theory can be tested in numerous ways. The simplest is probably to remove the borehole fluid from the simulation, but more practical tests could be performed. A more practical test would be an alteration of the tool design that would not only reduce the borehole background in simulation but also in practice. Such modifications could come in

the form of shielding portions of the detector that are surrounded mostly by borehole fluid (See Figure 7.) Another possibility is to use multiple detectors (Oleson), and to ignore counts from those detectors surrounded by borehole fluid. A final example would be to increase the far detector spacing, thereby reducing the probability of source neutrons reaching the detector through the fluid.

4.5.2 The Stranded Neutron Theory

An alternate theory is that the D-T neutrons indeed penetrate deeper into the formation, but there become stranded. This theory is supported mostly by arguments based on cross-section behavior. D-T neutrons penetrate more deeply because the cross-sections for important interactions are lower at fast neutron energies. Also, the inelastic and elastic scattering interactions that do occur at high energies are less likely to drastically change the neutron direction. High-energy neutron scattering is sometimes said to be forward-biased (See Figure 5.) As a source neutron initially loses energy in scattering events, it is most likely to be observed moving away from the detector. If it does eventually change directions and begin moving toward the detector, the loss of energy by the neutron has reduced the likelihood that it will traverse the distance back to the detector without becoming absorbed.

Using these arguments, an attempt to explain the lesser depth of penetration for the most penetrating source may be made. The initial interactions, where the neutron begins to slow, are of primary importance. If the neutron does not begin to lose energy near the tool, it is more likely to become stranded. The argument here boils down to claiming that the deeper penetration of the D-T source neutrons does not result in greater sensitivity to deeper regions of the formation, because the probability of registering a count is more strongly correlated with neutrons undergoing lethargy-gaining interactions early, while they are still close to the tool, than to any neutron interactions that occur deeper in the formation.

4.6 Conclusion

Interpretation of porosity logs taken with a Cf-252 radioisotope neutron source is not likely to be a problem, nor should the porosity logs taken with a D-T accelerator neutron source pose a problem of interpretation.

Further work in this area could include a deeper study of detector spacing effect with a more robust methodology. For a complete design, it would also be necessary to understand the effects of varying field conditions including borehole size, tool standoff, salinity, and matrix composition.

REFERENCES

Carter, L.L. and Cashwell, E.D. Particle Transport Simulation with the Monte Carlo Method, ERDA Critical Review Series. (1975.)

Duderstadt, James J. and Hamilton, Louis J. Nuclear Reactor Analysis. United States: John Wiley & Sons. (1976.)

Gardner, R.P. and Verghese, K. "Monte Carlo Nuclear Well-Logging Benhcmark Problems with Preliminary Intercomparison Results," Nuclear Geophysics 4. (1991.)

Knoll, Glenn F. Radiation Detection and Measurement, 3rd ed. United States: John Wiley & Sons. (2000.)

Koppel, J. U. and Houston, D.U. "Reference Manual for ENDF Thermal Neutron Scattering Data," General Atomics report GA-8744, Revised (1978.)

Marsh, J.W. et. Al. "High Resolution Measurements of Am-Be and Am-B Neutron Sources," Nuclear Instruments and Methods in Physics Research A, 366 (1995.)

Oleson, Jean-Rémy, et. al. "Wellsite Detection of Gas Reservoirs with Advanced Wireline Logging Technology", SPWLA 35th Annual Logging Symposium, (1994.)

Stacy, Weston M. Nuclear Reactor Physics. United States: John Wiley & Sons. (2001.)

X-5 Monte Carlo Team. MCNP—A General Monte Carlo N-Particle Transport Code, Version 5 3 vols. Oakridge, TN: Radiation Safety Information Computational Center. (2003.)